

Phase equilibria modeling in igneous petrology: use of COMAGMAT model for simulating fractionation of ferro-basaltic magmas and the genesis of high-alumina basalt

Alexei A. Ariskin *

Vernadsky Institute of Geochemistry and Analytical Chemistry, Russian Academy of Sciences, Kosygin st. 19, Moscow, 117975, Russian Federation

Received 21 September 1998; accepted 21 January 1999

Abstract

A new version of COMAGMAT-3.5 model designed for computer simulations of equilibrium and fractional crystallization of basaltic magmas at low to high pressures is presented. The most important modifications of COMAGMAT include an ability to calculate more accurately the crystallization of magnetite and ilmenite, allowing the user to study numerically the effect of oxygen fugacity on basalt magma fractionation trends. Methodological principles of the use of COMAGMAT were discussed based on its thermodynamical and empirical basis, including specific details of the model calibration. Using COMAGMAT-3.5 a set of phase equilibria calculations (called Geochemical Thermometry) has been conducted for six cumulative rocks from the Marginal Border Series of the Skaergaard intrusion. As a result, initial magma temperature ($1165 \pm 10^\circ\text{C}$) and trapped melt composition proposed to be parental magma to the Skaergaard intrusion were determined. Computer simulations of perfect fractionation of this composition as well as another proposed parent produced petrochemical trends opposite to those followed from natural observations. This is interpreted as evidence for an initial Skaergaard magma containing a large amount of olivine and plagioclase crystals (about 40–45%), so that the proposed and calculated parents are related through the melt trapped in the crystal–liquid mixture. This promotes the conclusion that the Skaergaard magma fractionation process was intermediate between equilibrium and fractional crystallization. In this case the classic Wager's trend should be considered an exception rather than a rule for the differentiation of ferro-basaltic magmas. A polybaric version of COMAGMAT has been applied for the genetic interpretation of a volcanic suite from the Klyuchevskoi volcano, Kamchatka, Russia. To identify petrological processes responsible for the observed suite ranging from high-magnesia to high-alumina basalts, we used the model to simulate the Klyuchevskoi suite assuming isobaric crystallization of a parental HMB magma at a variety of pressures and a separate set of simulations assuming fractionation during continuous magma ascent from a depth of 60 km. These results indicate that the Klyuchevskoi trend can be produced by $\sim 40\%$ fractionation of Ol–Aug–Sp \pm Opx assemblages during ascent of the parental HMB magma over the pressure range 19–7 kbar with the rate of decompression being 0.33 kbar/% crystallized (at 1350–1110°C), with ~ 2 wt.% of H₂O in the initial melt and ~ 3 wt.% of H₂O in the resultant high-Al basalt. © 1999 Elsevier Science B.V. All rights reserved.

Keywords: modeling fractionation; phase equilibria; tholeiitic trend; polybaric crystallization; decompression

* Tel.: +7-95-939-7071; Fax: +7-95-938-2054; E-mail: ariskin@geokhi.ru

1. Introduction

Problems of differentiation of basalt magmas constitute the core of igneous petrology, mostly due to the role of basalt parent in the generation of other magma types observed among plutonic and volcanic associations. Despite the great compositional diversity of igneous rocks, most of them have a basaltic precursor, therefore, a key aspect of understanding igneous differentiation processes is concerned with the mechanisms and conditions (P , T , f_{O_2} , P_{H_2O}) at which *primary* and *parental* basaltic magmas can generate derivative magmas resulting in the formation of tholeiitic, calc-alkaline, and other magmatic series. Bowen proposed *fractional crystallization* as a leading process responsible for the generation of chemical diversity and presented a set of petrological and phase equilibria arguments supporting this hypothesis (Bowen, 1928). He believed crystal settling to be the main physical mechanism causing separation of minerals from basaltic melts resulting in a specific compositional evolution called crystal fractionation. This mineral separation process accompanying with the chemical evolution is commonly combined under a general petrological term *magma fractionation*.

At present, magma fractionation is treated as a more complex event, often a combination of several physico-chemical processes, including those linked to heat-mass transfer and melting/crystallization, proceeding in igneous systems to different extents and open with respect to mantle, crustal or other magmatic material (DePaolo, 1981; O'Hara and Mathews, 1981; Grove et al., 1982; Kelemen, 1990; Nielsen, 1990; Cribb and Barton, 1996). Such a combined fractionation coupled with assimilation and/or mixing results in chemical consequences (differentiation), that cannot be reproduced or investigated by means of a physical experiment. To study these complex differentiation processes special numerical techniques need to be developed and applied (Frenkel et al., 1988a,b, 1989; Bergantz, 1995; Marsh, 1995; Ghiorso, 1997). The computational basis for this computer modeling should be sophisticated petrological models integrating in a single algorithm the solution of the equilibrium problem for crystallizing magmas and also dynamic considerations addressed to physical processes responsible for

the magma differentiation process (crystal settling, assimilation, magma chamber recharge, etc.). The number of such models in petrology still is not large, see review by Jaupart and Tait (1995). Probably, the *Convective–Cumulative model* of in situ differentiation is an example of the most comprehensive approach developed to describe and to solve relations between the dynamics of solidification fronts and fractional crystallization in sheet-like magma chambers (Frenkel et al., 1988b, 1989). Independently of igneous differentiation mechanism(s) and algorithm(s) used to link thermodynamic and dynamic parameters of magmatic differentiation, an important element of such physico-chemical models is the development of computer programs that allow one to calculate phase equilibria in closed magmatic systems at given external conditions.

The importance of phase equilibria controls on the fractionation and differentiation of magmas is due to the effect of crystallizing mineral compositions and proportions on *liquid lines of descent*. These mineral–melt equilibria dictate a general direction in which magma composition will evolve and define the dependence of chemical changes in the magmatic system upon P – T – f_{O_2} – P_{H_2O} conditions. Over the last 15 years, several thermodynamic and empirical models have been developed to simulate solid–melt equilibria for terrestrial magmas crystallizing in the compositional range from basalt to dacite (Nielsen and Dungan, 1983; Frenkel and Ariskin, 1984; Ghiorso, 1985; Ghiorso and Carmichael, 1985; Ariskin et al., 1987, 1993; Nielsen, 1990; Weaver and Langmuir, 1990; Longhi, 1991; Camur and Kilinc, 1995; Ghiorso and Sack, 1995; Yang et al., 1996).

However, despite the great efforts in the modernization of thermodynamic or empirical constraints, calibration techniques, and computational methods, serious problems continue to be encountered by petrologists in their attempts to apply these models to natural systems. Part of the problem is that these phase equilibria calculations still yield unsatisfactory results in the prediction of the calculated lines of descent, especially at elevated pressures and in the field of Fe–Ti oxide crystallization (Toplis and Carroll, 1996; Yang et al., 1996; Ghiorso, 1997). Another, no less important problem, is related to the methodological principles of these phase equilibria

models: a poor understanding of their thermodynamical and empirical basis, as well as calibration techniques, often results in poor results, which are sometimes ignored relative to the results of computer simulations.

The purpose of this paper is to present a new version of COMAGMAT, a package of petrological programs designed for simulations of equilibrium and fractional crystallization of mafic magmas (Ariskin et al., 1987, 1993). The most recent release of COMAGMAT (ver. 3.5) now includes new equations for the calculations of magnetite and ilmenite stabilities (Ariskin and Barmina, 1999). This allows the user to study more correctly the effect of oxygen fugacity on basalt magma fractionation trends. An example of such redox calculations will be given for the iron enrichment trend of the Skaergaard magma. Another example of the use of COMAGMAT includes identification of conditions of polybaric fractionation for high-magnesia magmas parental to the suite of high-alumina basalts from the Klyuchevskoi volcano, Kamchatka, Russia (Ariskin et al., 1995).

2. The COMAGMAT model

The COMAGMAT model is a computerized system designed for modeling magma crystallization and related processes occurring in volcanic and intrusion chambers at different depths and redox conditions. It was developed at the Vernadsky Institute (Moscow, Russia) and includes a series of linked programs constrained by over 20 years of field work, petrography, geochemistry, and computer simulation on the formation process of differentiated sills, layered intrusions as volcanic suites from Eastern Siberia, Karelia, Kamchatka, and other magmatic provinces (Frenkel et al., 1988a,b, 1989; Barmina et al., 1988, 1989a,b, 1992; Ariskin et al., 1988, 1990, 1995; Chalokwu et al., 1993, 1996).

The theoretical basis of these programs is an algorithm for modeling equilibrium and fractional crystallization of multiply saturated magmatic melts (Frenkel and Ariskin, 1984; Ariskin et al., 1993). It relies upon mineral–melt equilibria equations (geothermometers), which allow us to calculate crystallization temperatures and mineral compositions with a precision of 10–15°C and 1–3 mol.%, respectively

(Ariskin et al., 1987, 1993). The mineral–melt expressions have been derived for olivine (Ol), plagioclase (Pl), augite (Aug), pigeonite (Pig), orthopyroxene (Opx), titanium magnetite (Mt), and ilmenite (Ilm) from a large dataset of experiments covering the range from basalt to dacites.

The results of the program are in the form of calculated liquid lines of descent, plus the equilibrium mineral proportions and compositions. The phase equilibria calculations form the core of a model that allows the user to simulate processes ranging from simple isobaric crystallization to in situ differentiation processes resulting from crystal settling, and polybaric (decompression) fractionation—Fig. 1.

2.1. Thermodynamic background of COMAGMAT

Simulation of the course of crystallization of magmatic melts implies an ability to calculate mineral–melt equilibria at a given set of independent parameters of state, such as the pressure and temperature, or the bulk degree of crystallization. At constant pressure, this is known to be equivalent to the search for the minimum Gibbs free energy of the system (G). There are two main ways of approaching this problem. One is based on the algorithm of the minimization of G using a complex programming theory. The other is the iterative solution of a system of non-linear equilibrium equations and the mass action law using dependencies of equilibrium constants for each mineral–melt reaction on temperature and composition. Both approaches have strong thermodynamic justification and the main difference between them is that the former minimizes the Gibbs free energy in a direct form (e.g., Ghiorso, 1985; Ghiorso and Sack, 1995), whereas the latter implies that equilibrium constants are a function of G and temperature (Frenkel and Ariskin, 1984; Camur and Kilinc, 1995). In the COMAGMAT model we combined these basic thermodynamic considerations into a hybrid algorithm, which permits us to calculate phase equilibria step by step, as the total crystallization degree is increased (Ariskin et al., 1993).

2.1.1. Problem of the calculating melt component activities

The common thermodynamic basis of the above mentioned algorithms accounts for similar problems

geothermometers have been calibrated (Nielsen and Dungan, 1983; Weaver and Langmuir, 1990; Ariskin et al., 1993).

2.2. Calibration of the COMAGMAT model

During the development of COMAGMAT a great deal of experimental data on phase equilibria, major- and trace element partitioning, redox equilibria, as well as the effect of high pressures and water contents has been utilized. These data provides an empirical basis of this model which, in general, was compiled at the end of 1980. Our experience in practical applications of COMAGMAT and its additional testing on newly obtained experimental data indicate this model to fairly well predict low-pressure equilibria for silicate minerals. This is supported by recent results of independent calculations (Yang et al., 1996). Some problems with correct simulations of the appearance of Fe–Ti oxides have been overcome after recalibration of magnetite–melt and ilmenite–melt equilibria equations (Ariskin and Barmina, 1999). It is noteworthy that the flexible structure of COMAGMAT permits one to correct modeled temperatures within 10–20°C, adjusting

them to a selected set of ‘best’ experiments or to the data of petrological observations (Ariskin et al., 1993).

2.2.1. Mineral–melt geothermometers

The basic building blocks of the COMAGMAT model is a system of empirically calibrated equations that describe mineral–melt equilibria for Ol, Pl, Aug, Pig, and Opx (Table 1). Experimental data for these calibrations represent results of melting experiments published in 1979–1988 and include from 18 to 67 points for each mineral. All the experimental runs were carried out at 1 atm using the ‘Pt wire loop’ technique with controlled oxygen fugacities, for temperatures ranging from 1050 to 1300°C. The glass compositions were attained from mostly tholeiitic and mildly-alkaline systems, containing less than 4 wt.% Na₂O + K₂O.

A major problem in the use of these data for thermodynamic modelling is determining which experiments represent equilibrium compositions. There is a general consensus among experimentalists that run durations of no less than 48 h are necessary to achieve equilibrium between olivine or low-Ca pyroxene crystals and melt; for high-Ca pyroxene this

Table 1

Parameters of mineral–melt geothermometers used in the development of the basic version of COMAGMAT-3.0 phase equilibria model (Ariskin et al., 1993)

Mineral	Minal	Geothermometers	<i>n</i>	Reference
Olivine (Ol)	Fo	$\ln K = 5543/T - 2.32 + 0.210 \ln(\text{Al}/\text{Si})$	67	Ariskin et al., 1993
	Fa	$\ln K = 6457/T - 4.22 + 0.084 \ln(\text{Al}/\text{Si})$		
Plagioclase (Pl)	An	$\ln K = 10,641/T - 1.32 + 0.369 \ln R$	58	Ariskin and Barmina, 1990
	Ab	$\ln K = 11,683/T - 6.16 - 0.119 \ln R$		
Augite (Aug)	En	$\ln K = 8521/T - 5.16$	25	Ariskin et al., 1987
	Fs	$\ln K = 13,535/T - 9.87$		
	Wo	$\ln K = 2408/T - 1.24$		
	AlO _{1.5}	$D = 0.20$		
Pigeonite (Pig)	En	$\ln K = 8502/T - 4.74$	18	Ariskin et al., 1987
	Fs	$\ln K = 5865/T - 4.04$		
	Wo	$\ln K = 4371/T - 4.02$		
	AlO _{1.5}	$D = 0.10$		
Orthopyroxene (Opx)	En (11)	$\ln K = 7208/T - 3.71$	39	Bolikhovskaya et al., 1996
	Fs (12)	$\ln K = 6386/T - 4.39$		
	Wo (13)	$\ln K = 11,950/T - 10.40$		
	AlO _{1.5}	$D = 0.10$		

K—equilibrium constants, *D*—molar distribution coefficients, $R = \ln [(Na - K)Al/Si^2]$.

time should be increased in some extent, whereas for plagioclase run duration must be about 100–200 h to approach equilibrium (Grove et al., 1982; Grove and Bryan, 1983). For the above reason, we selected only those experiments that satisfy two constraints of run duration: $\tau \geq 96$ h for Pl, and $\tau \geq 48$ h for mafic minerals.

The calibration of the silicate geothermometers at a constant pressure was accomplished by the multiple regression in the form:

$$\ln K_i^j = a/T + b \ln R_L + c, \quad (1)$$

where j – mineral, i – mineral component (minal), K_i^j is equilibrium constant for the reaction of formation of this minal from melt components, R_L is a *melt structure-chemical parameter*, such as Si/O, Al/O, Al/Si; a , b , and c are the regression constants.

For the calculations of Fe^{3+} and Fe^{2+} species in silicate melts, we used the equations by Sack et al. (1980). Mineral component activities were assumed to be equal to the mole fractions of the cations in a single site (ideal solution). Assumption of this simple model means that the effects of non-ideality on mineral melt equilibria are attributed primarily to the liquid phase. To reduce the effects of the compositional dependence, a two-lattice model for melt component activities (Nielsen and Dungan, 1983) was used in the calibrations of mafic mineral geothermometers (Ariskin et al., 1987, 1993; Bolikhovskaya et al., 1996). The plagioclase–melt equilibria equations have been derived using a minor modification of the Nielsen's two lattice model (Ariskin and Barmina, 1990). Note, that inclusion of the melt structural-chemical parameters R_L as independent variables in Eq. (1) for Ol and Pl allowed us to significantly improve the fit to the experimental data.

When the regression parameters are calculated, one can test the statistics on goodness of the fit. The test procedure includes calculation of either $\ln K_i^j$ or $1/T$ for each liquid composition from the initial database and comparison between them and the experimental values. Comparison of the calculated and experimental temperatures for the calibration data set (Table 1) indicate an accuracy of 10–15°C (Ariskin et al., 1987, 1993). A similar comparison of calculated and experimental mineral compositions indicate

that Fo, An, En and Wo contents can be predicted on average within 0.5–0.7 mol% for Ol and 2–3 mol% for Pl and pyroxenes.

2.2.2. Using the INFOREX experimental database

To evaluate the specific COMAGMAT geothermometers we have also calculated the temperatures of appearance of Ol, Pl, Aug and Pig for the melt compositions from a set of experimental data that were not used in the basic calibration of these geothermometers. Those data were extracted from an experimental database, called INFOREX and developed in the middle of the 1990s for specialists dealing with thermodynamic processing of mineral–melt equilibria information (Meshalkin and Ariskin, 1996; Ariskin et al., 1996). Its major function is a computerized melting–experiment reference manual that presents data in a fixed format, with keyword search functions and flags as an integral part of the program. The INFOREX-4.0 database accesses information on 235 experimental studies carried out from 1962 to 1996 (Ariskin et al., 1997), including 8660 individual runs and more than 11,370 coexisting phase compositions for 36 minerals plus glass (Fig. 2).

Using searching and data management functions of INFOREX, four mineral–melt compositional files have been created: Ol–L ($n = 87$), Pl–L ($n = 95$), Aug–L ($n = 68$), and Pig–L ($n = 17$). These data files represent independent mineral–melt equilibria information published from 1989 to 1996, and satisfy the same constraints that were used during earlier basic calibrations. Results of comparisons show a good correlation of the COMAGMAT modeled temperatures with the those obtained from independent experiments (Fig. 3).

2.2.3. Fe–Ti oxides

In order to develop models simulating the crystallization of Fe–Ti oxides in natural lavas, we have processed published experimental data on magnetite–melt and ilmenite–melt equilibria (Ariskin and Barmina, 1999). About 62 Mt–melt and 75 Ilm–melt experiments were selected from the INFOREX-4.0 database on the basis of run time, melt composition and experimental technique. These data cover ranges of temperatures 1040–1150°C, oxygen fugacities of

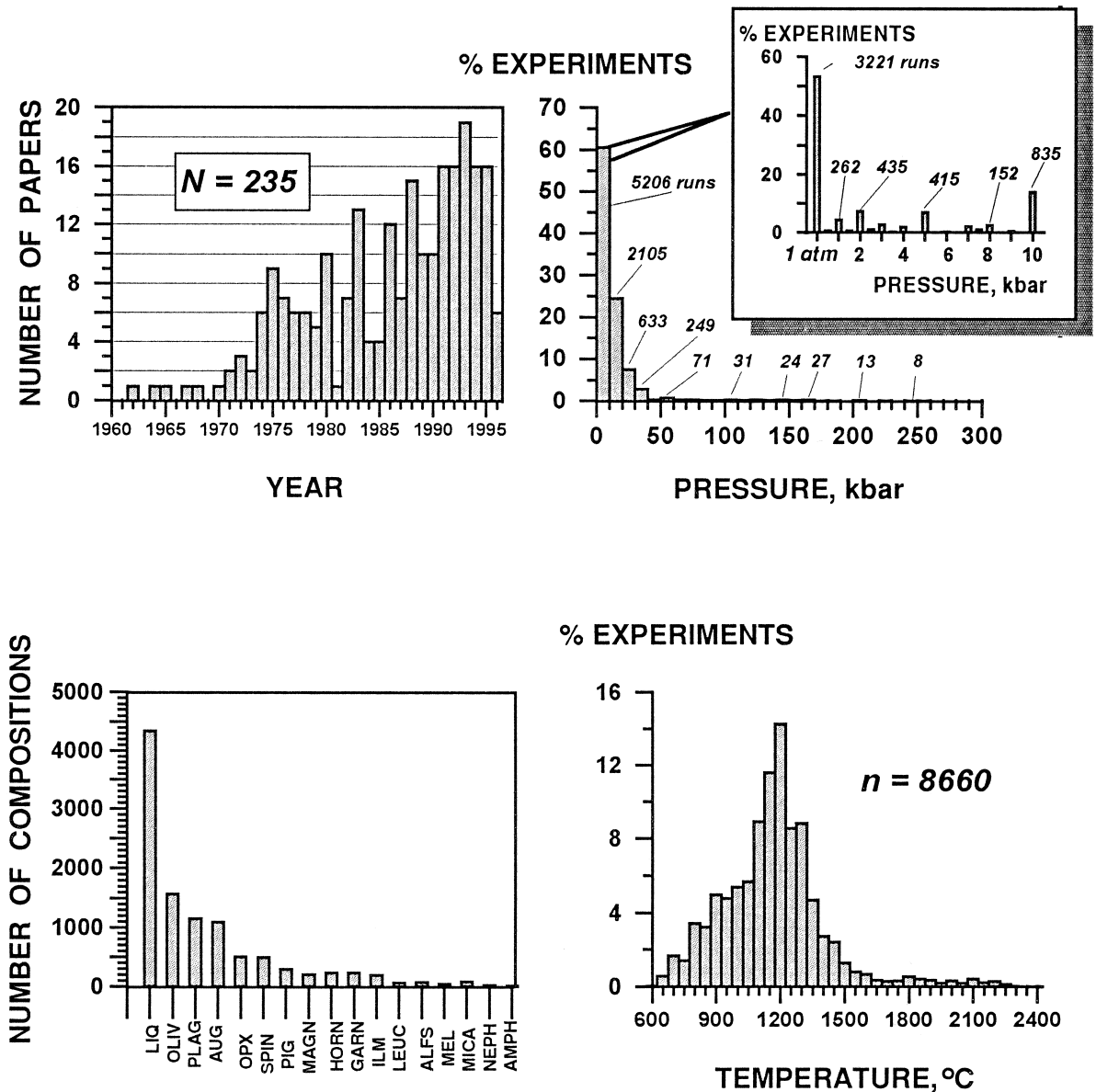


Fig. 2. Statistics on the experimental data available in the INFOREX-4.0 database (Ariskin et al., 1997). The primary INFOREX options include: (1) *System Configuration*, (2) *General Information*, (3) *Updating and Editing* data files, (4) *Selection of Run Conditions*, (5) *Setting Phase Assemblages* for the selected set of experiments, (6) *Export/Import* operations, (7) *Petrologic Calculations*, including the development of mineral–melt geothermometers, calculation of water contents in experimental glasses and projection of the experimental glass compositions onto ternary diagrams. An updated version of the INFOREX-4.0 database is available from the author on a request.

$10^{-13} < f_{O_2} < 10^{-6}$, and bulk compositions ranging from ferrobasalts to andesites and dacites. Five major cations (Fe^{3+} , Fe^{2+} , Ti^{4+} , Mg^{2+} and Al^{3+}) were

considered for the purpose of describing Fe–Ti oxide saturation as a function of melt composition, temperature and oxygen fugacity at 1 atm pressure. The

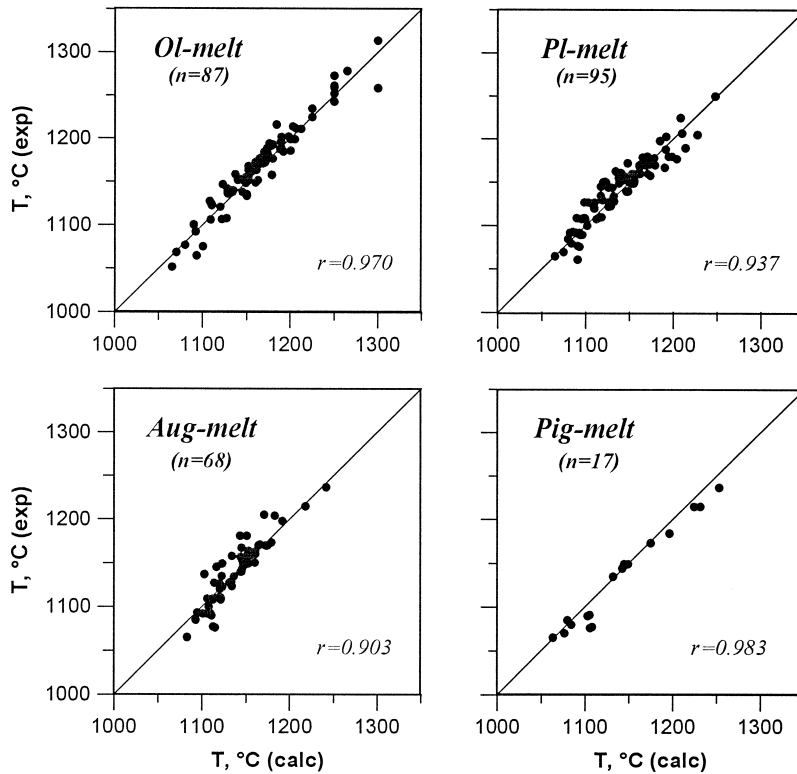


Fig. 3. Comparison of mineral crystallization temperatures observed in experiments with those calculated using mineral–melt geothermometers of COMAGMAT-3.0 for same liquid compositions. Experimental data were extracted from the INFOREX database (Ariskin et al., 1996, 1997) and include mineral–melt equilibria information published from 1989 to 1996, after the basic calibration of COMAGMAT was completed (Ariskin et al., 1987, 1993; Ariskin and Barmina, 1990).

empirically calibrated mineral–melt expression based on multiple linear regressions is:

$$\ln D_i^j = a/T + b \log f_{O_2} + c + d_1 x_{Na} + d_2 x_K + d_3 x_P, \quad (2)$$

where D_i^j is the molar distribution coefficient of the given cations between Mt or Ilm and melt; x_{Na} , x_K , and x_P are the molar fractions of Na, K, and P in the melt; d_1 , d_2 and d_3 are the regression coefficients (Ariskin and Barmina, 1999).

The empirically calibrated Mt–melt and Ilm–melt equilibria equations allowed us to develop two subroutines for calculating crystallization temperatures of the Fe–Ti oxides in mafic melts with an average accuracy of 15°C, and compositions with an accuracy of 0.5–2 mol%. Both subroutines have been

integrated into the COMAGMAT-3.5 program which now can be applied to magma compositions to numerically study the effects of oxygen fugacity on phase equilibria including Mt and Ilm. Results of testing this new model will be discussed in Section 2.4.

2.2.4. Calibrating the effect of elevated pressures

To develop a high pressure version of the COMAGMAT program, the empirical approach of Ariskin et al. (1990) based on the experimental data of Bender et al. (1978) was applied. They found that the pressure dependence of the crystallization temperatures $\partial T/\partial P$ for Ol and Pl were similar, and that the main result of increasing pressure was the expansion of the crystallization range for high-Ca pyroxene (Aug) relative to those of the other minerals.

This effect can be accounted for in the COMAGMAT model by adding to the ‘low-pressure’ Eq. (1) an empirical parameter β (cm³/mol) for each mineral component:

$$\ln K_i^j = (a + \beta)/T + b \ln R_L + c \quad (3)$$

Using the Bender et al. (1978) data, and the low-pressure mineral–melt geothermometers (Table 1), we selected empirical values of β for Ol, Pl, and Aug. The results that fit the data with the least error were obtained using the optimal parameters of $\beta_{\text{Fo,Fa}}^{\text{Ol}} = 1.2$, $\beta_{\text{En,Fs,Wo}}^{\text{Aug}} = 1.4$, $\beta_{\text{An}}^{\text{Pl}} = 1.0$, and $\beta_{\text{Ab}}^{\text{PL}} = 2.0$ cm³/mol, with Al₂O₃ in augite increasing by 0.7 wt.%/kbar. Application of this pressure correction reproduced the input data within 15–30°C from 1 atm up to 15 kbar.

The absence of well defined parameters β for low-Ca pyroxenes and Fe–Ti oxides permits the user to apply the high-pressure COMAGMAT model to systems where crystallization of these minerals did not play a significant role. For example, results of applications of this version to MORB compositions indicate COMAGMAT accurately predicts phase equilibria at 4 kbar (Yang et al., 1996). At higher pressures of 12–15 kbar, the use of this model may result in a shift of the calculated Aug boundaries of 2–3 kbar at the same temperature, or 15–30°C at the same pressure. Nevertheless, petrological analysis of these high pressure calculations provides useful insight into the effect of pressure on liquid lines of descent in natural systems (Ariskin et al., 1990). An example of such polybaric simulations will be shown for the fractionation of high magnesia magmas of the Klyuchevskoi volcano, Kamchatka, Russia (see Section 4).

2.2.5. Calibrating the effect of water contents

To account for the effect of water on mineral–melt equilibria calculated with COMAGMAT a simple semi-empirical approach has been used (Almeev and Ariskin, 1996). This approach includes: (1) the development of an empirical equation describing water solubility in basaltic to granitic melts as a function of temperature, pressure, and melt composition; (2) application of this equation to water-saturated experimental glasses extracted from the INFOREX database; (3) using this ‘hydrous’ experimental in-

formation for the calculation of correction coefficients which could be used to correct mineral–melt equilibria temperatures computed for the water-saturated glasses as per ‘dry’ conditions; (4) integration of these correction coefficients into COMAGMAT to model changes in phase boundaries due to the presence of water in magmatic melts.

The main effect of water on phase equilibria in magmas is related to a differential decrease of mineral crystallization temperatures. This results in relative changes in the appearance of minerals on the liquidus, shifting phase boundaries, and changes in the compositional evolution of the liquid phase. As a first approximation, the temperature effect may be accounted by means of the following expression:

$$T_{\text{H}_2\text{O}}^j = T_{\text{dry}}^j - \lambda_j C_{\text{H}_2\text{O}}, \quad (4)$$

where $T_{\text{H}_2\text{O}}^j$ and T_{dry}^j are j -mineral saturation temperatures in a hydrous and dry melt, $C_{\text{H}_2\text{O}}$ is the water content in the melt (wt.%), λ_j (°C/wt.% H₂O) is a correction coefficient. The λ values for each mineral may be calculated from experimental data in hydrous systems, providing the water content in the melt is known:

$$\lambda_j = [T_{\text{H}_2\text{O}}^{j(\text{exp})} - T_{\text{dry}}^{j(\text{calc})}] / C_{\text{H}_2\text{O}}, \quad (5)$$

where $T_{\text{H}_2\text{O}}^{j(\text{exp})}$ is the experimental temperature for a solid–melt assemblage including j -mineral, $T_{\text{dry}}^{j(\text{calc})}$ is j -mineral crystallization temperature calculated using low-pressure geothermometers from Table 1 calibrated for dry conditions and pressure dependence parameters β (see Eq. (3)). To accomplish the goal, one can use data of more than 2000 water saturated experiments available in the INFOREX-4.0 database: glass compositions are available for as many as 500 of them (Ariskin et al., 1997). The main problem in the use of this information for the calibration of a hydrous version of COMAGMAT is the fact that direct analytical information on the water contents in the experimental glasses is practically absent.

2.2.5.1. Calculating water solubility. To produce useful, if empirical constraints, we used 79 water solubility (mostly superliquidus) experiments to develop a purely empirical equation which can be

applied to a wide range of systems, from basalts to granites (Almeev and Ariskin, 1996):

$$\begin{aligned} \ln C_{\text{H}_2\text{O}} = & 4.39 + [38,483(\text{Si}/\text{O}) - 14,710]/T \\ & + 0.59 \ln P - 21.45(\text{Si}/\text{O}) \\ & + 3.89(\text{Al}/\text{Si}), \end{aligned} \quad (6)$$

where $C_{\text{H}_2\text{O}}$ is water content in the silicate liquid (wt.%), P is total pressure (bars), T is temperature, and Si/O and Al/Si are atomic ratios in the glasses. The data on which Eq. (6) was calibrated cover the range of pressures 0.2–9 kbar and temperatures 800–1200°C (Hamilton et al., 1964; Kadik et al., 1971; Sisson and Grove, 1993a,b; Dixon et al., 1995) with an internal precision of 0.32 wt.% for H_2O content and 0.25 kbar for the pressure.

2.2.5.2. Calculation of correction coefficients λ_j . Using the search procedures of INFOREX we selected water saturated subliquidus experiments conducted with basalts and andesites at pressures up to 10 kbar. The compositions of experimental glasses were grouped by the presence of a particular mineral in the observed phase assemblage (e.g., for Ol such assemblages included Ol + L, Ol + Pl + L, etc.). Thus, four compositional data sets were compiled: Ol–melt (69 runs), Pl–melt (81), Aug–melt (56), and Opx–melt (19). For each experimental point the H_2O content in the melt was estimated using Eq. (6), and mineral crystallization temperatures were calculated using the ‘dry’ high-pressure version of COMAGMAT. The calculated temperatures are 100–300°C higher than the respective ‘wet’ experimental temperatures: this difference was normalized to the

estimated water content as per Eq. (5). The calculated average values of λ_j are summarized in Table 2 and have been also integrated into the COMAGMAT-3.5 model.

2.2.6. Trace-element partitioning

With the exception of Cr, trace-element contents in basaltic melts are known to have little influence on the liquidus temperatures and composition of the major mineral phases. Therefore, trace-element partitioning calculations can be separated from the phase equilibria calculations. This does not mean that major- and trace-element systematics are not to be linked, only that the major-element phase equilibria can be calculated independently of trace-element contents. To accomplish this goal, we use the traditional approach to the description of mineral–melt partitioning in the form of the weight single-component distribution coefficients D_i^j (Barmina et al., 1989a, 1992). Calculation of the major-element mineral–melt equilibria controlled parameters, such as temperature and fractionating or melting mineral proportions, allows us to constrain the trace-element systematics, stated as the trace-element concentrations in the liquid and solid phases:

$$C_i^l = \frac{C_i^0 M_0}{\left(M_L + \sum_{j=1}^m D_i^j M_j \right)}, \quad C_i^j = D_i^j C_i^l, \quad (7)$$

where C_i^0 is the initial bulk content of i element in the molten system, M_0 mass of the system, M_L and M_j are current masses of the melt and solid phases,

Table 2

Correction coefficients to dry mineral–melt temperatures used in the development of the hydrous version of the COMAGMAT-3.5 model

P (kbar)	Ol	Aug	Opx	Pl
1	17.9 ± 6.0 (14)	34.3 ± 7.1 (12)	22.4 ± 3.4 (2)	59.6 ± 7.8 (23)
2	18.7 ± 2.9 (21)	24.8 ± 2.2 (19)	22.3 ± 1.2 (4)	49.9 ± 4.2 (18)
2.5		23.7 ± 3.9 (3)		47.6 ± 1.0 (3)
3			18.3 (1)	43.1 ± 1.5 (23)
4				38.3 ± 1.6 (3)
5	10.2 ± 5.5 (3)	15.5 ± 3.3 (8)		38.1 ± 3.1 (6)
6.9				37.8 ± 0.6 (5)
7.5	5.1 ± 3.7 (3)	14.5 ± 1.6 (4)	12.5 ± 2.2 (4)	
10	1.3 ± 0.7 (2)	10.5 ± 1.1 (5)	9.3 ± 1.0 (4)	

The number of points is given in the parenthesis.

with all masses calculated as part of the COMAGMAT program. The use of partitioning expressions that have been empirically corrected for compositional dependences, temperature and pressure provides us with a more accurate means of describing trace-element behavior. At present, the COMAGMAT-3.5 model provides the option of simulating the evolution of trace-element trends for the two following groups: (1) Mn, Ni, Co, Cr, Sc, V, Sr, Ba, Rb, Cu, and (2) La, Ce, Nd, Sm, Eu, Gd, Dy, Er, Yb, Lu (Ariskin et al., 1993).

2.3. Structure of the COMAGMAT model

Details of the algorithm used to constrain the COMAGMAT model are described by Ariskin et al. (1993). The core of the model is the integration of several iteration loops including *Thermometry*, *Equilibration* and *Melting / Crystallization* constraints which allow us to solve the equilibrium problem at a given crystallinity of the modeled system. These main iteration loops interact to simulate the course of equilibrium crystallization for natural cotectic assemblages step by step, as the total mode of crystals is increased (Fig. 4).

As documented from the flowchart, the initial conditions and simulation subroutines for the COMAGMAT program are contained in a series of setup files. These eight data files include the desired model parameters (MAINMENU.DAT), initial major- and trace-element contents (COMMAJ.DAT and COMTRA.DAT), distribution coefficients for trace elements (DICOEF.DAT), parameters of the mineral–melt geothermometers (MINERS.DAT), oxygen buffers (OXYBUF.DAT), the regression coefficients to correct calculated temperatures (CORRECT.DAT) as well as some dynamics parameters for modeling in situ differentiation (INTRUS.DAT).

The modeling process starts from a completely molten system ($\varphi_{\text{cr}} = 0$) and may be conducted with a crystallization increment $\Delta\varphi_{\text{cr}} = 1\text{--}2$ mol% up to the bulk system crystallinity $\varphi_{\text{cr}}^{\text{max}} = 80\text{--}90\%$. After the calculations are complete, the information will be written to an output file as a sequence of several tables containing phase proportions and compositions as a function of the total crystallinity, plus the equilibrium temperature defined for each step. To simulate fractional crystallization or in situ magma

differentiation process a dynamic block called *INTRUSION* has been included in the algorithm (Ariskin et al., 1993).

2.3.1. Main functions of COMAGMAT

The COMAGMAT programs operate under DOS on IBM compatible computers and include four main routines that may be used in solving common petrological problems (Fig. 1): (1) *Thermometry of Mineral–Melt Equilibria*, (2) *Simulating Equilibrium Crystallization*, (3) *Simulating Fractional Crystallization*, and (4) *Simulating Layered Intrusion Formation*. The first option allows one to calculate mineral–melt equilibria temperatures for melt compositions that are supposed to be saturated with a mineral. As shown in Fig. 4, this thermometry function is an important part of the general algorithm used to simulate the course of magma crystallization. The following two functions are addressed to simple crystallization process, which can be modeled in the *isobaric* or *polybaric* mode for systems open or closed with respect to oxygen. Note, that the *Decompression Crystallization* is modeled with COMAGMAT by means of the monotonic decrease of total pressure from an initially given value P_{max} to a final value P_{min} with a constant negative pressure increment ΔP per step of crystallization. Such a crystallization process results in specific liquid lines of descent that differ considerably from those calculated at isobaric conditions (Ariskin et al., 1995).

The *Simulating Layered Intrusion Formation* function was designed in the form of the *INTRUSION* subroutine to model complex magma differentiation processes proceeding in closed magma chambers (Frenkel et al., 1988a,b, 1989). This algorithm includes a linkage between crystallization, crystal settling, vigorous convection, mineral accumulation, and thermal history in the magma chamber (Ariskin et al., 1993; Chalokwu et al., 1996). It allows the user to study a diversity of liquid lines of descent related to both *perfect* and *partial* fractionation (Maaloe, 1976), as well as crystallization *intermediate* between equilibrium and fractional processes.

2.4. Verification of the COMAGMAT model

The best way to test phase equilibria models is to compare modeled and experimental trajectories of

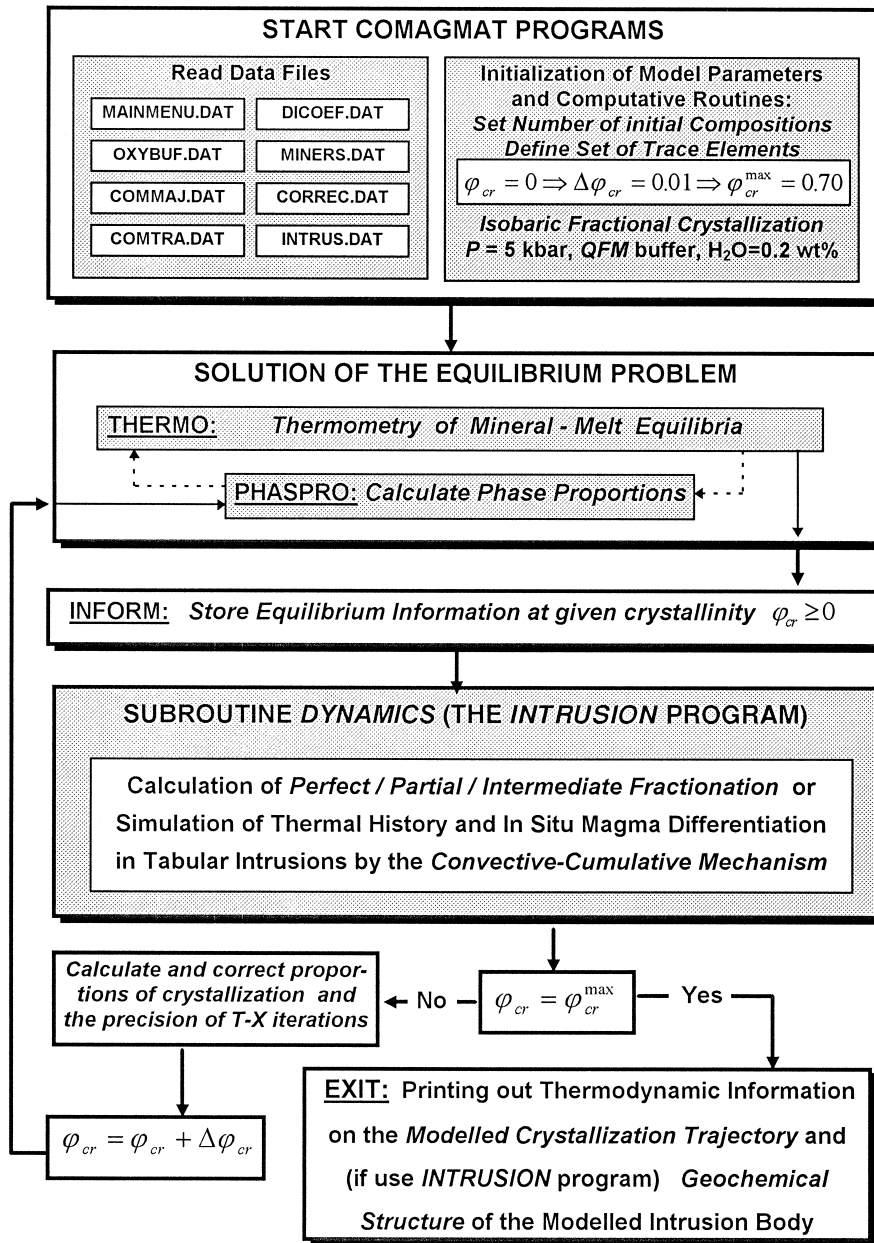


Fig. 4. General flowchart of the COMAGMAT-3.5 model. This scheme demonstrates that switching on the dynamic calculations (including the fractionation algorithms) is organized to be after the equilibrium problem is solved at a given degree of crystallization.

equilibrium crystallization for the same initial liquid compositions. Despite the fact that most of experimental data represent melting experiments, the bulk composition of the experimental starting material

may be considered as the initial liquid composition for the following phase equilibria simulations. To perform this comparative computations we used the *Simulating Equilibrium Crystallization* option of

Table 3

Compositions of basalts used in experimental studies and testing COMAGMAT calculations for tholeiitic systems at 1 atm pressure

Plot in Fig. 4	1	2	3	4	5	6
Study	Walker et al., 1979	Grove and Bryan, 1983	Tormey et al., 1987	Grove et al., 1990	Snyder et al., 1993	Yang et al., 1996
Starting material	MORB basalt V30-RD8-P12	Magnesian tholeiite ALV-528-1-1	Magnesian tholeiite AII78-3-102	MORB basalt ALV-1690-20	Ferrobasalt 4-3	Low-Na Mg-tholeiite RE-46
SiO ₂	48.73	49.60	48.80	50.00	47.40	48.80
TiO ₂	1.21	0.67	0.96	1.66	2.27	0.62
Al ₂ O ₃	16.19	16.00	17.50	15.70	14.20	15.40
FeO	9.29	9.57	9.58	10.20	14.34	8.91
MnO	0.18	0.16	0.14	0.14	0.20	0.16
MgO	8.05	10.40	9.62	7.78	6.13	10.70
CaO	12.43	11.90	10.20	11.00	9.04	13.50
Na ₂ O	2.24	1.74	2.71	3.07	2.97	1.55
K ₂ O	0.35	0.10	0.11	0.13	0.70	0.01
P ₂ O ₅	0.00	0.00	0.00	0.16	0.22	0.03

COMAGMAT-3.5 with the crystallization increment $\Delta\varphi_{cr} = 1$ mol%, calculating the course of equilibrium crystallization up to the bulk crystallinity $\varphi_{cr}^{max} = 70\%$.

2.4.1. Testing 1 atm calculations

Six different tholeiitic compositions from six experimental studies were selected to test COMAGMAT calculations at 1 atm and dry conditions

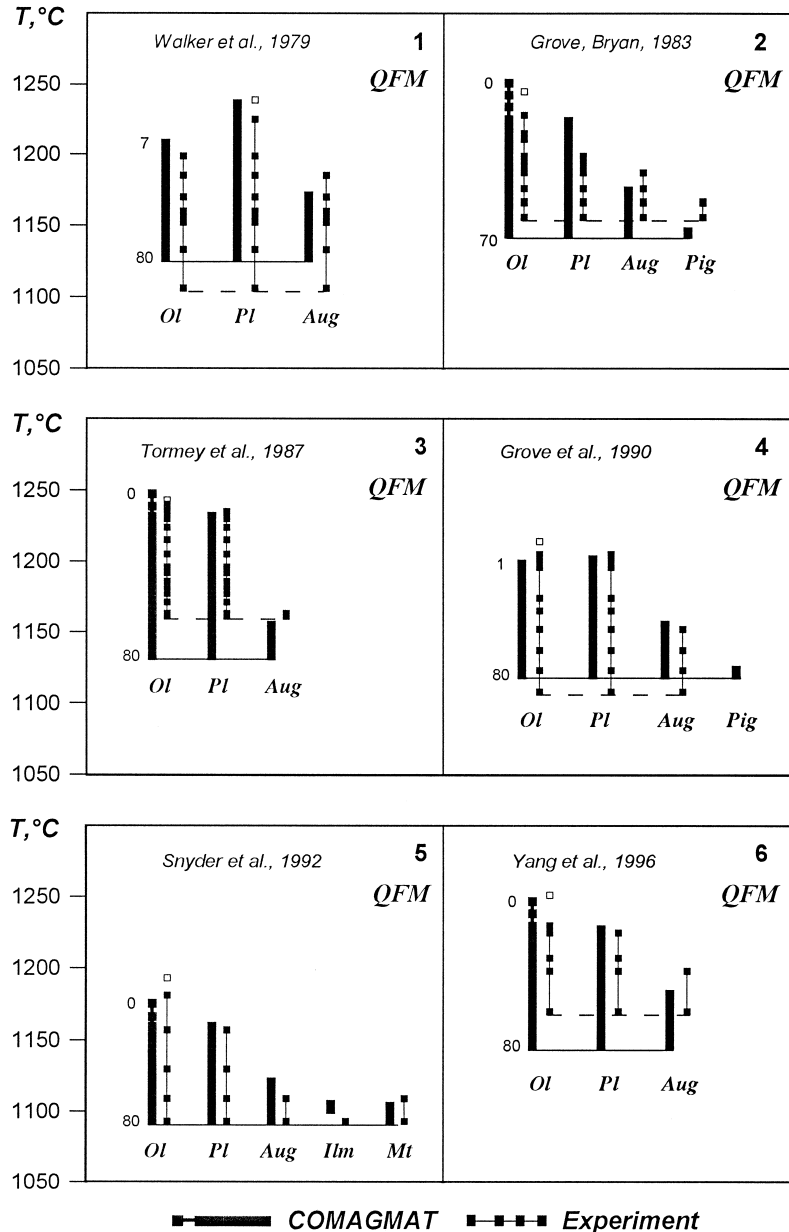


Fig. 5. Comparison of experimental and calculated equilibrium liquidus relations of selected tholeiitic compositions. Numbers of plots correspond to the starting materials in Table 3. Calculations were carried out at 1 atm with the use of the COMAGMAT-3.5 phase equilibria model.

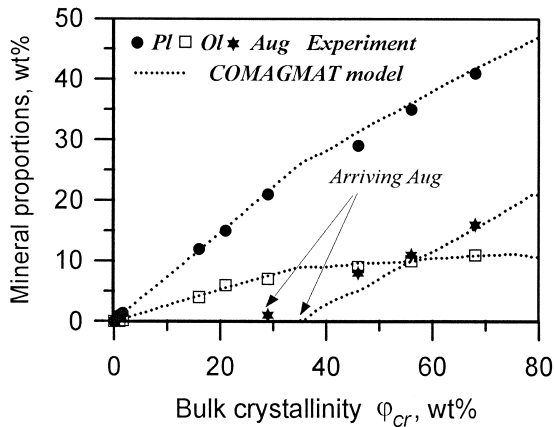


Fig. 6. Modeled and experimental evolution of phase proportions during equilibrium crystallization of a tholeiitic basalt (Grove et al., 1990). Results of this modeling correspond to the crystallization sequence 4 in Fig. 5.

(Walker et al., 1979; Grove and Bryan, 1983; Tormey et al., 1987; Grove et al., 1990; Snyder et al., 1993; Yang et al., 1996). All of the experiments were carried out near the QFM buffer and cover the range of temperatures 1050–1260°C. Compositions of these starting materials (initial melts) are listed in Table 3. Results of comparisons of the modeled data with those obtained in experiments are displayed in Figs. 5–7.

Six plots in Fig. 5 demonstrate that the COMAGMAT model fairly well predicts the crystallization sequences in the tholeiitic systems: with the exception of the first Al and Ca enriched composition (Walker et al., 1979), appearance of the minerals on the liquidus corresponds to the order $Ol \pm Pl \rightarrow Aug \rightarrow Pig \rightarrow oxides (Mt \pm Ilm)$. Deviations of the calcu-

lated mineral crystallization temperatures from experimental values do not exceed 10–15°C. Note, that for the fifth composition (Snyder et al., 1993) COMAGMAT adequately ‘felt’ the saturation with magnetite and ilmenite at late stages of crystallization.

2.4.1.1. Crystallization proportions. Direction of liquid lines of descent during magma crystallization process is known to depend mostly on the proportions between crystallizing minerals. For this reason, the accuracy of the calculated mineral crystallization proportions is the most important criteria of the validity of any phase equilibria model. Earlier versions of COMAGMAT have demonstrated that this model accurately reproduced proportions of the $Ol-Pl$ cotectics estimated from optical observations (Bender et al., 1978). A further impression of the accuracy of COMAGMAT can be obtained from comparisons of the modeled phase proportions with those found from mass-balance constraints based on experimental phase compositions (Fig. 6). These plots give evidence that COMAGMAT correctly predicts mineral proportions for the crystallizing $Ol-Pl-Aug$ assemblage (Grove et al., 1990). Average mineral crystallization proportions for six modeled tholeiitic compositions are listed in Table 4.

2.4.1.2. Liquid lines of descent. If the crystallization sequence, mineral compositions, and phase proportions were calculated with a good accuracy, chemical evolution of the liquid phase will also be predicted correctly. This is due to conservation of mass of chemical components in the modeled closed system. As an example, two sets of liquid lines of descent

Table 4

Average mineral crystallization proportions calculated with COMAGMAT for the equilibrium assemblages shown in Fig. 5

Starting composition in Fig. 4	Crystallization proportions, wt. %			
	$Ol-Pl$	$Ol-Pl-Aug$	$Ol-Pl-Aug-Pig$	$Ol-Pl-Aug-Mt$
1	29.0–71.0	6.6–44.3–49.1	–	–
2	31.7–68.3	7.7–41.8–50.5	(–2.5)–40.7–51.8–10.0	–
3	29.1–70.9	9.1–43.9–47.0	–	–
4	26.4–73.6	5.5–46.2–48.3	(–13.3)–43.3–53.3–16.7	–
5	26.4–73.6	7.8–43.2–49.0	–	(–12.9)–35.4–58.0–19.5
6	32.1–67.9	7.4–41.6–51.0	–	–

Negative values for Ol indicate a peritectic reaction with the dissolution of this mineral during equilibrium crystallization.

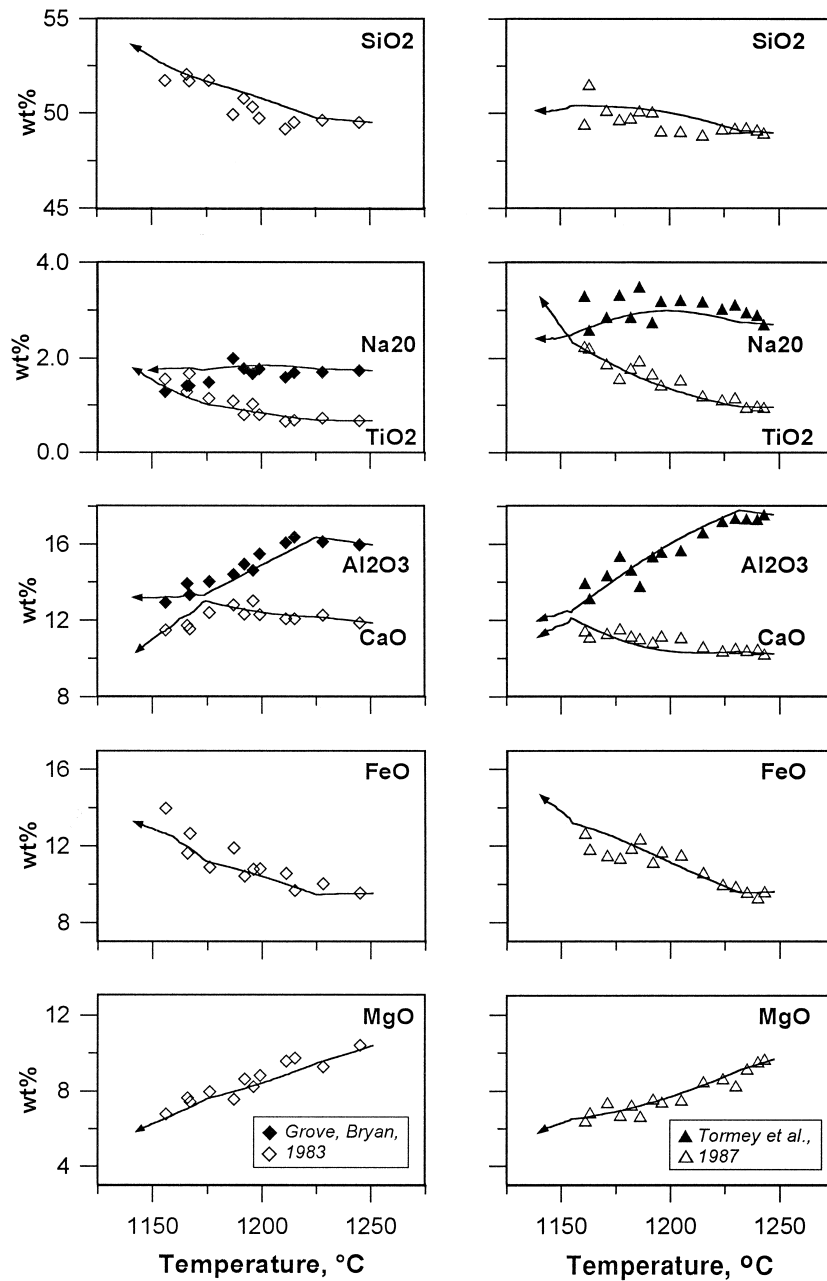


Fig. 7. Comparison of modeled liquid lines of descent with those observed in experiments (Grove and Bryan, 1983; Tormey et al., 1987). Results of this modeling correspond to the crystallization sequences 2 and 3 in Fig. 5.

attributed to the calculated trajectories 2 and 3 in Fig. 5 are compared with those from melting experiments (Grove and Bryan, 1983; Tormey et al., 1987) in Fig. 7. These results suggest that for the calculated

temperature-compositional trends are close to the experimental dependencies. This gives us confidence that chemical trends calculated with COMAGMAT might be useful in petrological interpretations based

on the genetic analysis of variation diagrams for natural systems.

2.4.2. Testing Mt stability calculations

As mentioned above, the most recent modifications of COMAGMAT are concerned with the integration of new Mt- and Ilm-models (Ariskin and Barmina, 1999). To test more carefully the magnetite model, we used experimental results by Hill and Roeder (1974), which are independent of the new calibration. The authors presented data on the stability of Ti-magnetite in a ferrobasic system (sample GL-RHB) at 1 atm in a wide range of oxygen fugacities $-14 < \log f_{O_2} < -0.68$ (Fig. 8). Using the new COMAGMAT-3.5 model, a series of calculations simulating the course of 1 atm equilibrium crystallization has been conducted for the range $-10 < \log f_{O_2} < -6$, with GL-RHB composition as the starting composition.

These calculations were carried out at five oxygen fugacities ($\log f_{O_2} = -6, -7, -8, -9, \text{ and } -10$) with the crystallization increment of 1 mol%, up to 1100°C. The modeled results are shown in Fig. 8 and demonstrate that this modeling realistically repro-

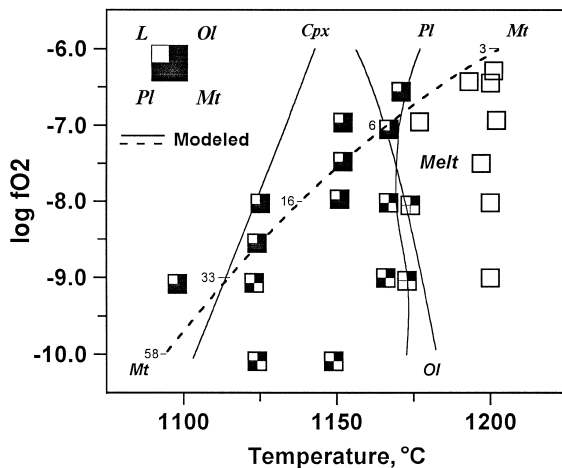


Fig. 8. Comparison of experimental phase assemblages produced during equilibrium crystallization of a ferrobasic melt (Hill and Roeder, 1974) with those calculated using COMAGMAT-3.5 (Ariskin and Barmina, 1999). To minimize the effect of errors in the calculated silicate minerals temperatures on the stability of magnetite, those temperatures were increased by 15°C for Ol and 10°C for Pl. Numbers adjacent to the Mt saturation line indicate X_{Uiv} in magnetite calculated from Stormer (1983).

duces crystallization sequences observed in the independent experiments. Magnetite was calculated to be the first phase to crystallize at $f_{O_2} = 10^{-6}$ bar, and the fourth phase crystallizing at $f_{O_2} = 10^{-9}$ bar. Calculated Mt crystallization temperatures differ from those observed in experiments by no more than 10–15°C, i.e., within the accuracy of the proposed model. Note, the dependence of the calculated Mt liquidus on oxygen fugacity changes with f_{O_2} : 30–35°C/ $\log f_{O_2}$ at $-7 < \log f_{O_2} < -6$, and 15°C/ $\log f_{O_2}$ at $\log f_{O_2} < -10$. Accounting for the average temperature precision of the Mt model of 15°C, one can guess that in practical calculations, a shift of 0.5–1 log units may be observed in the $T - \log f_{O_2}$ diagrams for the calculated Mt stability field.

2.4.3. Testing calculations in hydrous systems

During the process of phase equilibria calculations in hydrous systems H_2O is considered to be an excluded (incompatible) component, completely partitioned in the liquid. In fact, the presence of water in the system is only implied: this component does not affect mineral component activities, so that the silicate part of the melt evolves as if it is a dry system. The enrichment of this *implicit component* in the melt can proceed up to the level corresponding to the water solubility limit at a given pressure, see Eq. (6). So the influence of H_2O on the calculated phase equilibria is accounted for only by means of decreasing mineral crystallization temperatures in accordance with Eq. (4) and correction coefficients listed in Table 2 (Almeev and Ariskin, 1996). Such a simplified, if somewhat primitive, approach allows one to study general features of magma crystallization in the presence of water, e.g., the decrease in Pl crystallization field with increasing water content resulting in the enrichment of the melt with Al_2O_3 (Ariskin et al., 1995).

An example of such calculations is displayed in Fig. 9, which is the projection of the compositions of multiply saturated melts onto the OLIV–PLAG–CPX diagram (Tormey et al., 1987; Grove, 1993). Two modeled lines in this plot represent results of equilibrium crystallization calculations conducted in anhydrous and hydrous conditions at 2 kbar with a high alumina basalt (HAB) as starting composition. Phase relations of this HAB (sample 79–35 g) have been

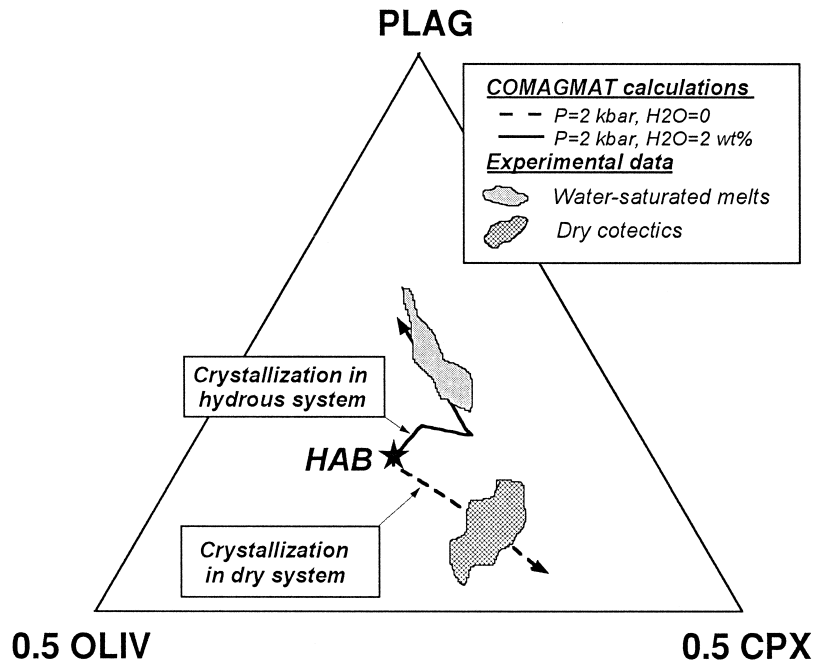


Fig. 9. Comparison of modeled dry and hydrous liquid lines of descent with the compositions of multiply saturated melts observed in anhydrous and water-saturated experiments. Starting composition HAB represent a high-alumina basalt studied experimentally at 2 kbar water pressure (Sisson and Grove, 1993a,b). The field of dry cotectics was constructed from experimental glass compositions corresponding to Ol + Pl + Aug ± Mt ± Pig + L assemblages (extracted from the INFOREX database). Calculations with COMAGMAT-3.5 program simulate equilibrium crystallization of HAB at 2 kbar in the absence of water and at 2 wt.% H₂O in the initial melt. The projection method is after (Tormey et al., 1987; Grove, 1993).

studied under the water pressure of 2 kbar field (Sisson and Grove, 1993a): experimentally obtained compositions of these water-saturated glasses are shown in Fig. 9. The lower field represents 41 experimental glass compositions corresponding to Ol + Pl + Aug ± Mt ± Pig + L assemblages, observed at 2 kbar and anhydrous (dry) conditions. These experimental data were extracted from the INFOREX-4.0 database (Ariskin et al., 1997).

One can see that the projection of the 'dry' modeled liquid line of descent onto the diagram demonstrates a common evolution toward the field of anhydrous cotectics, whereas the evolution of a hydrous liquid line of descent with initial H₂O content of 2 wt.% results in the alumina-enriched water-saturated cotectics observed in the experiments (Sisson and Grove, 1993a). It is interesting to note, that the calculated temperatures for the water-saturated melts (1022–1058°C) are close to those observed in experiments (1000–1050°C), with the calculated H₂O

content in the melt ranging from 5.98 to 6.27 wt.% (Almeev and Ariskin, 1996).

2.5. General notes to the use of COMAGMAT

Similar to other phase equilibria models, COMAGMAT has an internal general temperature precision of about 10–20°C, which is slightly different for various minerals and depends upon the compositional range under investigation. In many cases, such precision provides realistic reproduction of the crystallization sequences and liquid lines of descent, especially for magnesian initial compositions with a wide field of stability for Ol + L and Ol + Pl + L assemblages. If the initial melt is close to simultaneous saturation with several phases (e.g., Ol + Pl + Aug + Pig + Mt + L), this simulation can result in overestimated temperatures for one or two phases, which may differ by 20–30°C due to the differences in the calculated temperatures, even within the common error (e.g., +10°C for Pl and –20°C for Ol).

To account for these problems we developed a simple procedure to correct the calculated temperatures by means of setting a temperature shift for each particular mineral at the initial stage of the calculations, see CORREC.DAT file (Fig. 4). Given the possibility of systematic compositional dependencies in the calculated temperatures, a special FUNLIQ subroutine has been included in the COMAGMAT model which is linked with the CORREC.DAT file (Ariskin et al., 1993).

Thus, the first advice: do not hurry to conclude that COMAGMAT is incorrect if during test calculations the calculated crystallization sequences are found to differ from those you expected from a set of experimental data or petrological observations. Instead, try to understand the reason for these differences by setting small temperature shifts for different minerals or by slightly changing the pressure, redox conditions or water content in the melt.

The second advice: we strongly recommend that COMAGMAT be paired with the INFOREX experimental database (Ariskin et al., 1997). The INFOREX system includes an ability to create mineral–melt equilibria datafiles for a given range of compositions and conditions (Meshalkin and Ariskin, 1996; Ariskin et al., 1996). Those files can be further imported to COMAGMAT to test mineral–melt equilibria temperatures (see Fig. 1) in order to estimate the presence of a systematic shift for a particular mineral. These shifts can be set into the CORREC.DAT files to be used in further calculations.

The third advice: before starting petrological calculations, try to model the whole crystallization sequences available in the INFOREX database for the compositional range of interest. Often, an additional small shift of the calculated temperatures is necessary to best fit the experimental data for these particular compositions. To conclude, the COMAGMAT model works best for tholeiite-like systems (Figs. 5–7), however, accounting for the above recommendations, it may be also applied to mildly-alkaline and calc-alkaline basalts and andesites.

3. Simulating the effect of magnetite fractionation in ferro-basaltic magmas

Even after decades of investigation, debate surrounding the role of magnetite crystallization in the

differentiation of basalt magmas remains one of the most active in igneous petrology. This problem is directly related to genetic interpretations of silicic differentiates, which are important members of both tholeiitic and calc-alkaline series. Most workers today agree that the andesite/diorite to rhyolite/granophyre magmas originate by fractionation of a basalt parent, however, there is a controversy about redox conditions and the dominant phases controlling the covariation of iron and silica in the melt (Babansky et al., 1983; Ghiorso and Carmichael, 1985; Grove and Kinzler, 1986; Kadik et al., 1986, 1990; Hunter and Sparks, 1987; Ariskin et al., 1988; Shi, 1993; Sisson and Grove, 1993a,b; Snyder et al., 1993; Thy and Lofgren, 1994; Toplis and Carroll, 1996; Ariskin, 1998). A key aspect of this discussion is the relative role of magnetite and silicate mineral crystallization in the formation of the observed series of magmas. Both mechanisms have been proposed, specifically, after experimental demonstrations that increasing f_{O_2} will stabilize the magnetite field in basaltic systems, causing marked SiO_2 enrichment in the liquid (Osborn, 1959; Presnall, 1966; Egglar and Osborn, 1982), whereas changes in phase proportions of olivine, plagioclase, and pyroxenes again generate a derived suite of more silica enriched magmas both at 1 atm (Shi, 1993) and at elevated pressures (Grove and Kinzler, 1986). In this section, we will demonstrate the use of COMAGMAT in the numerical study of the effect of Mt fractionation on the liquid lines of descent originated from a ferro-basalt parent at low pressure and under both open and closed conditions with respect to oxygen. As a model example, the differentiation of a parental Skaergaard magma will be included in these considerations.

3.1. Problems of differentiation of iron-enriched tholeiitic magmas

A distinguishing feature of the tholeiitic differentiation trend is a stepwise enrichment of residual melts in iron oxides during the early and middle stages of fractionation, followed with a marked depletion at the late stage. There is a general consensus that this enrichment with FeO_{tot} is due to the low-pressure fractionation of basaltic magmas, where plagioclase is a predominant phase in the crystalliz-

ing mineral assemblages, such as Ol–Pl and Ol–Pl–Px \pm Mt (e.g., Grove and Baker, 1984; Ariskin et al., 1988). Main discussions are concerned with (1) the highest possible extent of the iron enrichment, (2) direction of the SiO₂ evolution (enrichment or depletion), and (3) the relative contributions of silicate phases and magnetite to these major-element signatures.

3.1.1. Mass balance constrains from the Skaergaard intrusion

Using data on the relative volumes and average compositions of cumulates from the Skaergaard intrusion, Wager with colleagues calculated compositions of residual melts approximating the chemical evolution of a parental tholeiitic Skaergaard magma during intrachamber differentiation processes (Wager and Deer, 1939; Wager and Brown, 1967). According to these mass balance constraints, while the intrusion solidification degree F ranges from 0 to 88 wt.%, the calculated compositional series demonstrates a monotonous increase in the sum of iron oxides FeO_{tot} from 9.6 to 18.2 wt.%, with a complimentary decrease of SiO₂ from 48.1 to 46.9 wt.%.

The late stages of crystallization 88 < 98% are characterized by a small increase in FeO_{tot} up to 21.7% and SiO₂ up to 49.8%, followed by a decrease in the concentration of iron oxides and the formation of very unusual ferro-dioritic compositions. At $F = 99.3\%$, the calculated differentiates contained 18.5 wt.% FeO_{tot} and 55.0 wt.% SiO₂ (Fig. 10). This mass balance derived chemical evolution has been considered by several generations of petrologists as a typical example of tholeiitic basalt magma fractionation, which corresponds to the high iron enrichment (Fenner's) differentiation trend. Similar estimates of the compositions of derivative melts have been obtained for some other mafic layered intrusions, e.g., Kiglapait (Morse, 1981).

Paradoxically, although highly Fe-enriched compositions containing up to 18–19 wt.% FeO_{tot} have been encountered in basalts and natural glasses (e.g., Brooks et al., 1991), no volcanic equivalents of the calculated ferro-diorites as the terminal products of the Skaergaard magma differentiation have been found. It might be also noted that the majority of tholeiitic volcanic series display a moderate enrichment in FeO, usually up to 13–15% while exhibiting no decrease in SiO₂ (Osborn, 1979).

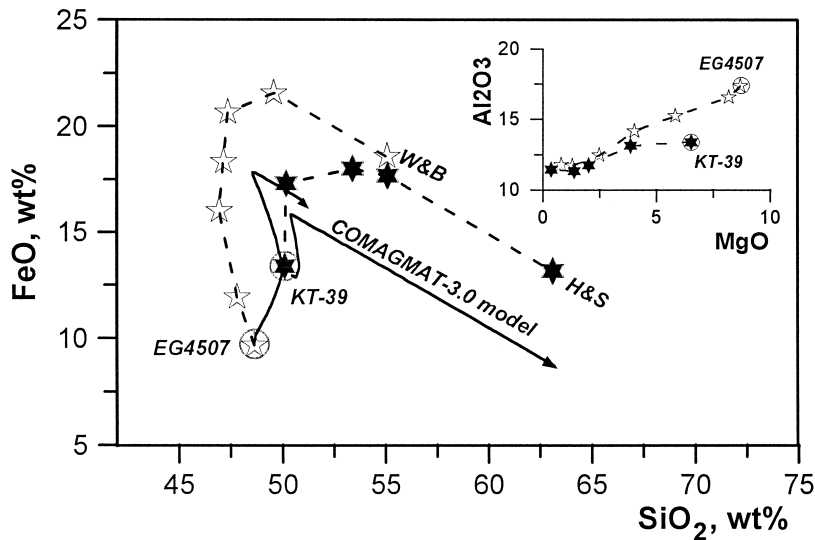


Fig. 10. Differentiation trends for two magmas proposed to be parental to the Skaergaard intrusion. The initial compositions correspond to chilled marginal gabbro-EG4507 (Wager and Brown, 1967) and KT-39 (Hoover, 1989). Mass-balance calculated trends: W & B (Wager and Brown, 1967); H & S (Hunter and Sparks, 1987). Phase equilibria modeled trends represent results of calculations of fractional crystallization of EG4507 and KT-39 with the use of earlier versions of COMAGMAT (Ariskin et al., 1988, 1993). These calculations were carried out in the vicinity of QFM buffer, with the increment of crystallization 1 mol%. The modeled Mt crystallization temperatures were increased to 40°C so that it can better fit the experimental data by Hoover (1989) for QFM buffer.

3.1.2. The effect of redox conditions (experimental constrains)

Probably, Osborn (1959) was the first petrologist to provide a phase equilibria interpretation for these observations. Based on the results of melting experiments within the MgO–FeO–Fe₂O₃–SiO₂ system, he established that similar shifts in the direction of liquid lines of descent are due to different proportions of magnetite fractionation, which, in turn, are controlled by the redox conditions. It was found that upon closed-system crystallization (with the bulk Fe³⁺/Fe²⁺ ratio being constant), fractionation of Mt does not cause the melt to be depleted in FeO_{tot}, whereas if the system is open with respect to oxygen ($f_{O_2} = \text{const}$), the content of iron oxides in the melt drops rapidly after the onset of magnetite crystallization (Osborn, 1959, 1979).

Petrogenetic considerations of these chemical features led Osborn to the conclusion that intra-chamber differentiation processes for tholeiitic magmas (in particular, for the Skaergaard magma), may probably occur in a closed system, whereas the fractionation of magmas parental to volcanic suites takes place under a certain oxygen pressure (Osborn, 1959, 1979). This conclusion was also supported by experiments with synthetic (Presnall, 1966; Egglar and Osborn, 1982) and natural (Babansky et al., 1983; Kadik et al., 1986; Snyder et al., 1993; Thy and Lofgren, 1994; Toplis and Carroll, 1995) basaltic to andesitic systems.

3.1.3. Revised direction of the Skaergaard magma fractionation

A new surge of petrological interest to this problem was triggered after the publication by Hunter and Sparks (1987). These authors presented a set of mass-balance and phase equilibria arguments that cast doubt on the reality of the calculated trend of the Skaergaard magma differentiation (Wager and Deer, 1939; Wager and Brown, 1967). It was shown that the principal contradiction of the Wager's mass-balance approach lies in the fact that this classical trend of super-enrichment with FeO_{tot} accompanied by a monotonous decrease in silica (Fig. 10) is inconsistent with the available estimates of the parental Skaergaard magma composition (sample EG4507, 48.1 wt.% SiO₂) and experimental data on

phase equilibria for mafic magmas (Hunter and Sparks, 1987, 1990). This high iron enrichment versus silica depletion trend appears to be difficult (if not impossible) to correlate with the low SiO₂ contents (44–46%) in the crystallization products of the 'gabbroic assemblage' Ol–Pl–Aug ± Mt. Another discrepancy with available experimental data is that the calculated inflection point at which the iron enrichment is changed to the silica enrichment does not coincide with the appearance of Fe–Ti oxides, which are known to appear quite early in the Skaergaard Layered Series (Wager and Brown, 1967; McBirney, 1989, 1996).

Thus, it was suggested (Hunter and Sparks, 1987, 1990) that the differentiation of the Skaergaard magma is actually an example of a common tholeiite-magma evolution similar to that observed among volcanic suites in Iceland: ferro-basalt → andesite-basalt → icelandite (ferro-andesite) → dacite (Carmichael, 1964). During the early stages, this fractionation process was caused by the crystallization of the Ol–Pl ± Aug assemblage, causing the melt to be monotonously enriched in FeO_{tot}, with the SiO₂ content being roughly constant in the range 50–52 wt.%. The appearance of Mt at later fractionation stages caused the melt to be strongly depleted in iron, accompanied by the complementary enrichment in SiO₂. These speculations were supported by simple mass-balance calculations, including subtraction of specified amounts of the Skaergaard gabbroic components from the proposed parental magma (Hunter and Sparks, 1987), see the H&S trend in Fig. 10.

It is noteworthy that the proposed method of calculating compositions of magma differentiation products based on the successive subtraction of the gabbroic components (Hunter and Sparks, 1987) has the same drawback as Wager's approach. The use of the observed intrusive rock compositions in mass-balance calculations does not allow one to account for the possible presence of a trapped melt in the cumulates, as well as the potential existence of suspended crystals in the main magma body. From this point, phase equilibria calculations simulating the course of fractional crystallization may provide more petrological information on the differentiation of ferro-basalt magmas (Ariskin et al., 1988; Toplis and Carroll, 1996).

3.2. Computer simulations of the Skaergaard magma fractionation

One of the main consequences of the Hunter and Sparks's interpretation was relatively high SiO₂ contents in magmas crystallizing gabbroic assemblages which gave rise to the cumulates of the Lower Zone of the Skaergaard intrusion (50–52 wt.%). This suggestion was based on the summary by Biggar (1983) who has reviewed data on experimental phase equilibria including Ol + Pl + Cpx assemblages, as well as petrological observations for some volcanic suites. Accounting for magnetite (+ Ilm) precipitation after appearance of clinopyroxene in the Skaergaard crystallization sequence, this could mean that Fe–Ti oxides also crystallized from the melts containing no less 50–52 wt.% SiO₂. This was opposite to the W&B differentiation trend (Fig. 10). To study this problem numerically we have conducted a series of calculations simulating the course of fractional crystallization for a proposed parental Skaergaard magma under open and closed conditions with respect to oxygen at 1 atm total pressure (Ariskin et al., 1988).

3.2.1. First calculations in open and closed with respect to oxygen systems

These calculations were carried out using the TOLEMAG program (Ariskin et al., 1987) which is a precursor of COMAGMAT (Ariskin et al., 1993). The chilled marginal gabbro EG4507 was used as an initial composition (Wager and Brown, 1967), with the redox conditions varied in the range from QFM to IW (iron–wüstite buffer). In general, these simulations realistically reproduced the observed Skaergaard crystallization sequence: Ol + Pl → Ol + Pl + Aug → Ol + Pl + Aug + Mt ± Pig, with the exception that Ilm was crystallized only at the most reduced conditions of the IW buffer.

What was important is that all of the calculated trends indicated a marked increase in the silica content in the melt during fractionation of the 'troctolitic' Ol + Pl assemblage, up to ~ 50 wt.% SiO₂—the inflection point where Aug began to crystallize. Similar results representing a renewed set of calculations with COMAGMAT-3.0 (Ariskin et al., 1993) at the QFM oxygen buffer are displayed in Fig. 10. These recent simulations were conducted with two compositions proposed to be parental to the Skaer-

gaard suite—EG4507 and KT-39 (Hoover, 1989; McBirney, 1996). According to these calculations, both samples are Ol + Pl cotectics within 10°C, with liquidus temperatures of ~ 1240°C (EG4507) and 1170°C (KT-39). They are characterized by the appearance of high-Ca clinopyroxene as a third crystallizing phase, with a pronounced FeO_{tot} enrichment up to the point where Mt began to crystallize. Despite an older magnetite crystallization model used in the COMAGMAT-3.0 (Ariskin et al., 1993), the simulated phase equilibria showed the compositional evolution of the Skaergaard magma to be more complex than can be inferred from simple mass-balance calculations (Wager and Brown, 1967; Hunter and Sparks, 1987). For the further considerations (see Section 3.4) it is also important that the observed compositional differences between samples EG4507 and KT-39 might be linked by the fractionation (or accumulation!) of Ol and Pl crystals—Fig. 10.

Probably, the most interesting result of the earlier simulations by Ariskin et al. (1988) was the recognition that the crystallization proportions for Mt in the closed O₂ system were calculated to be 1.5–2 lower compared with those for the open (buffered) O₂ system. This resulted in changes in the extent of iron enrichment, similar to that demonstrated recently in the modeled FeO–SiO₂ diagrams by Toplis and Carroll (1996).

3.2.2. Simulations by Toplis and Carroll (1996)

Based on the results of their previous experimental studies of phase equilibria in a synthesized ferro-basalt system, Toplis and Carroll (1995) developed a semi-empirical model, including known phase relations, mineral–melt partitioning information, and mass-balance constraints. This model was used to elaborate the consequences of equilibrium and fractional crystallization for natural ferro-basaltic systems both open and closed to oxygen. Overall, results of these simulations supported data of previous modeling (Ghiorso and Carmichael, 1985; Ariskin et al., 1988) that in a system open with respect to oxygen Mt saturation "leads to strongly decreasing iron and increasing silica contents of residual liquids, whereas systems closed to oxygen crystallize less abundant magnetite, leading to a less pronounced iron depletion in the liquid".

The starting composition on which this model was calibrated (Toplis and Carroll, 1995) and for which these comprehensive phase equilibria were calculated, represents a synthetic analog of a dike rock adjacent to the Skaergaard intrusion (Brooks and Nielsen, 1978) and close in the bulk composition to the KT chilled marginal gabbro (Hoover, 1989; McBirney, 1996). So, it was not a surprise that the modeled liquid lines of descent (Toplis and Carroll, 1996) were found to be similar to those calculated with COMAGMAT and shown in Fig. 10, in that none of them reproduced the classical trend proposed by Wager and Brown (1967). Both models were calibrated on independent experimental data sets and use different computational algorithms, and it would thus be imprudent to assume that the calculated chemical trends are not correct. Note also, that these models predicted limit of iron enrichment < 20 wt.% FeO_{tot} .

3.3. Discussion of the Skaergaard differentiation trend

This attempt to revise traditional views on the evolutionary trend of the Skaergaard magma could not but provoke a controversy among petrologists who, to this day, have not resolved the contradictions between the geological and mineralogical arguments put forward by opponents of the new interpretation (McBirney and Naslund, 1990; Morse, 1990; Brooks and Nielsen, 1990) and the results of the above mentioned calculations (Hunter and Sparks, 1987, 1990; Ariskin et al., 1988; Toplis and Carroll, 1996). In this context, it is especially difficult to interpret experimental data by McBirney and Naslund (1990), who presented a set of liquid compositions preserved as an interstitial material in the cumulative rocks they crystallized (Fig. 11). The liquid compositions were obtained after melting experiments carried out on the rocks of the Skaergaard Layered Series and display an increasing enrichment in FeO_{tot} and the depletion in SiO_2 , until a field of immiscibility is reached (McBirney and Nakamura, 1974). This experimental trend for cumulative rocks from the Lower and Middle Zones corresponds well to that proposed by Wager and Brown (1967), and followed from co-magmatic dike compositions (Brooks and Nielsen, 1978).

Moreover, these compositions demonstrate that such relatively low silica liquids could be in equilibrium with the observed ‘gabbroic’ assemblages, including Ti-magnetite as a principal mineral. This is important to note, as far as Hunter and Sparks (1987, 1990) believed that the crystallization of $\text{Ol} + \text{Pl} + \text{Cpx} \pm \text{Mt}$ assemblages could proceed only from the melts containing 50–52 wt.% SiO_2 (Biggar, 1983). We have conducted a special search through the INFOREX database, in order to find experimental glass compositions corresponding to the equilibrium with the $\text{Ol} + \text{Pl} + \text{Aug}$ assemblage (\pm oxides) in natural systems. At least 50 glasses containing 45–49 wt.% SiO_2 , mostly at 15–18 wt.% FeO were identified in the library of experiments. Most of these compositions include 3.5–5 wt.% TiO_2 and might be addressed to Fe–Ti basalts (Brooks et al., 1991), so that one can conclude that Wager’s and McBirney’s trends in fact do not conflict with the phase equilibria information.

Thus, the main problem of the Skaergaard magma fractionation may be formulated as follows: how is it that commonly used petrological techniques give rise to liquid lines of descent opposite to those found in phase equilibria simulations? Before trying to answer this question, let us apply the COMAGMAT model to get an independent estimate of whether or not the parental melt compositions used in these simulations were correct (Ariskin et al., 1988; Toplis and Carroll, 1996).

3.4. Estimates of the Skaergaard parental magma composition

First of all note, that the use of the term ‘parental magma’ in petrology is often of dual meaning, in its application to mafic layered intrusions or differentiated sills. Assuming a parental magma to be free of suspended (intratelluric) crystals, that magma should be considered a pure liquid. Otherwise (more typically for natural processes), the parental magma should be considered as a mixture of an initial (parental) magmatic melt and crystal material, representing a *primary mineral assemblage* (Marsh, 1989; Chalokwu et al., 1993). For the further considerations, we will distinguish between the *parental melt* and *parental magma*, implying that the term ‘magma’ is addressed exclusively to a heterogeneous

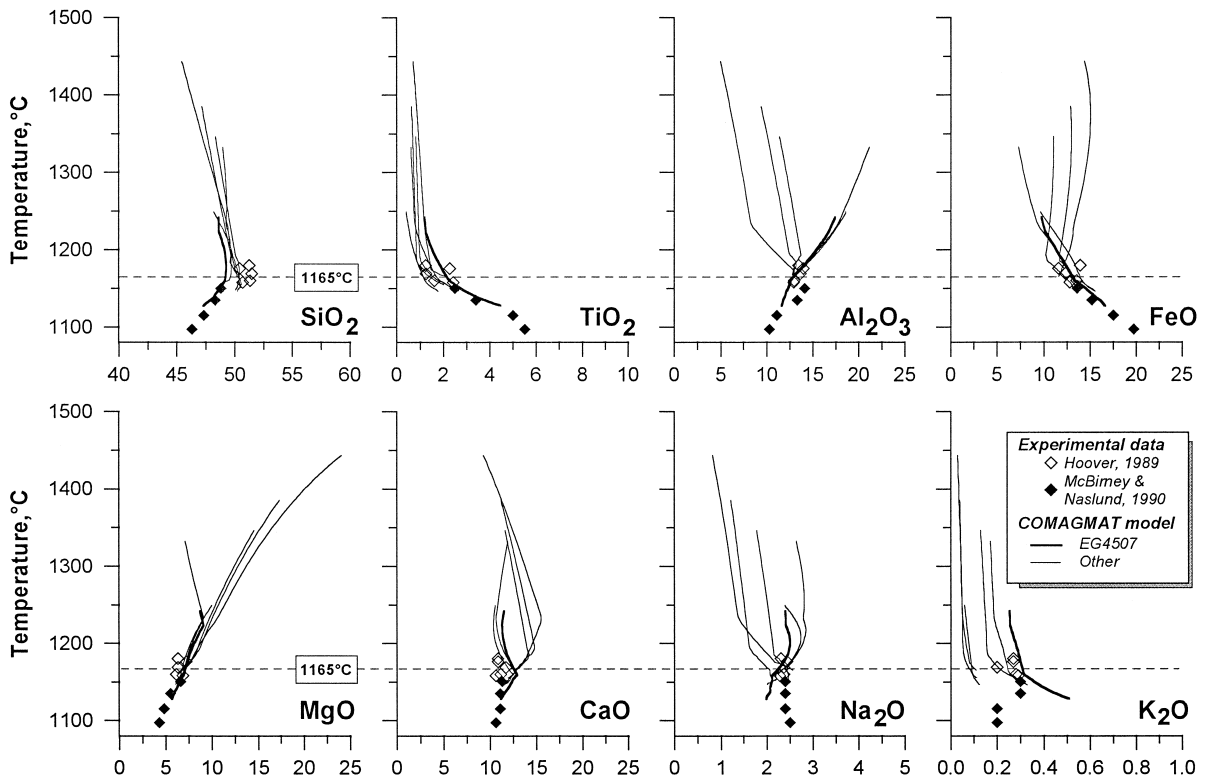


Fig. 11. Calculated and experimental liquid lines of descent assumed to present the evolution of melts trapped in the Skaergaard cumulates. Open diamonds represent the experiments carried out on the Marginal Border Series pristine cumulates (Hoover, 1989). Filled diamonds correspond to trapped melts obtained in the melting experiments with cumulates from the Lower and Middle Layered Series (McBirney and Nakamura, 1974; McBirney and Naslund, 1990). Lines represent results of simulations of equilibrium crystallization of melts for six marginal cumulates (initial compositions see Table 5). These calculations were conducted with the COMAGMAT-3.5 model (Ariskin and Barmina, 1999; this paper) at 1 atm and QFM conditions. The temperature $1165 \pm 10^\circ\text{C}$ is assumed to indicate the primary equilibrium temperature for the trapped melt.

system, whereas the parental melt is to represent a liquid part of the igneous phase assemblage.

Probably, to accurately approach the parental magma composition it is necessary to calculate an average intrusion composition, weighted in accordance with the spatial distribution and density of the rocks composing the intrusive body. This approach works perfectly well for documented vertical sections of tabular bodies, such as differentiated traps (Frenkel et al., 1988b, 1989; Barmina et al., 1989a). Unfortunately, due to a varied (often unknown) intrusion form, these calculations could not be applied to large layered complexes. It forces petrologists to pay more attention to parental melt compositions,

which may also provide an important insight into the prior fractionation and differentiation processes of magma chambers.

The classic petrological–geological approach of defining a parental melt composition is based on the use of bulk analyses representing fine-grained lithologies (assumed to be chilled) from the margins of layered intrusions (e.g., Wager and Brown, 1967). Such an approach is known to be effective if the margin rocks experienced insignificant changes in their composition due to thermal and chemical contact processes. With the purpose of defining such non-altered rocks, which also do not contain accumulated minerals, Hoover (1989) undertook a detailed

petrographic and geochemical screening of over 80 specimens from several contacts of the Skaergaard intrusion. Finally, he presented a set of samples (chilled marginal gabbro) found commonly within 1 to 3 m of the exposed intrusive contact and having uniform ferrobaltic compositions (e.g., sample KT-39 in Table 5, Fig. 10). The liquidus phase relations of the KT-39 sample investigated experimentally at 1 atm were consistent with the sequence of cumulus minerals observed within the Marginal Border Series and the Layered Series (Hoover, 1989). As an independent test of the parental melt composition, Hoover (1989) performed a few additional melting experiments on cumulates, which represent the earliest and the less fractionated rocks crystallized within the Marginal Border Series. The purpose of these experiments was to define liquid compositions which could resemble melts trapped in the cumulates. The partial melt compositions observed in the range of temperatures of 1110–1180°C were, in general, close to the chilled marginal gabbro, such as KT-39 (Table 5). A problem in the petrological interpretation of these data is related to a disagreement between glass compositions obtained in similar melting experiments conducted with cumulates from the Lower Zone of the Layered Series (McBirney and Nakamura, 1974; McBirney and Naslund, 1990). Both sets of the experimental glass compositions are displayed in the temperature–composition diagrams in Fig. 11.

Below, we will present results of phase equilibria calculations carried out with COMAGMAT for several cumulates from the Marginal Border Series. These calculations are also intended to define the trapped liquid compositions with the purpose of interpreting relations between the experimental glass compositions (Hoover, 1989; McBirney and Naslund, 1990) and to provide an independent estimate of the trapped (parental?) Skaergaard melt.

3.4.1. Method of Geochemical Thermometry

Geochemical Thermometry is a technique designed for solving inverse problems of igneous petrology targeted at extracting genetic information, such as the temperature, trapped liquid and primary mineral compositions as well as primary phase proportions, as ‘recorded’ in the whole-rock chemical compositions (Frenkel et al., 1988a,b; Barmina et al.,

1989a,b; Chalokwu et al., 1993). This method is based on the premise that any crystal–liquid mush (e.g., cumulates), before complete crystallization, will pass through a stage when relative movements of accumulated crystals and trapped liquid have ceased. In this case, the primary phase proportions and compositions would determine the bulk chemical composition of rocks crystallized later in situ from the initial magmatic mixture. Considering a single rock, for which its primary cumulative assemblage was in equilibrium with a trapped liquid, one can expect that the path of equilibrium (closed system) crystallization for this ‘numerically molten’ rock must pass through the point (melt composition) corresponding to this primary equilibrium. If the temperature of this equilibrium was known independently, it would be possible to define the trapped liquid composition as a melt corresponding to this temperature.

As a rule, the primary temperature is unknown, so that even possessing information on the temperature–composition dependence of the melt evolution does not allow one to determine the primary liquid unambiguously. This is absolutely the same problem as was encountered by experimentalists after melting experiments with the Skaergaard cumulates (Fig. 11). This ‘temperature’ problem, however, may be solved, if after petrological studies two or more orthocumulates were identified to have originated from a single primary cumulus assemblage. If these cumulates have contrasting chemical compositions with the differences caused by simple variations in the proportions of accumulated crystals (e.g., Ol and Pl), one can state that calculating two or more equilibrium crystallization trajectories inevitably will result in the compositional lines intersecting in the T – X spacing. In such a case, the cluster in T – X space of the concentrations of 10 major plus trace elements will determine the initial (parental) liquid composition, its primary liquidus temperature, as well as phase proportions, including the amount of trapped liquid (Frenkel et al., 1988a,b).

The Geochemical Thermometry technique involves computer modeling of the course of equilibrium crystallization for several igneous rocks which are assumed to represent the same primary mineral–melt assemblage, followed by a procedure of comparisons and searching for the intersection of the calculated liquid lines of descent in the T – X space

Table 5

Compositions of pristine marginal cumulates used for Geochemical Thermometry as well calculated, experimental and naturally observed compositions proposed to be parental to the Skaergaard magmatic melts

Description	Pristine marginal cumulates from Hoover (1989)					Chilled gabbro (Wager and Brown, 1967) EG4507 ?	Trapped liquid (= parental melt ?)		Chilled gabbro (Hoover, 1989) KT-39 0.5
	Sample Distance (m)	UT-04 2.5	UT-08 8.5	EC-10 1.0	MEO-10 3.0		KT-47 6.0	Calculated at 1165°C	
SiO ₂	44.65	48.38	46.92	47.45	48.19	48.08	50.01 (0.42)	51.30	49.69
TiO ₂	0.69	0.60	0.63	0.40	0.81	1.17	1.68 (0.33)	1.61	2.66
Al ₂ O ₃	4.88	20.91	9.36	18.32	11.37	17.22	12.95 (0.07)	12.99	13.21
FeO _{tot}	14.16	7.19	12.84	9.49	11.04	9.63	13.24 (0.51)	13.55	12.76
MnO	0.24	0.10	0.10	0.15	0.19	0.16	0.19 (0.05)	0.26	0.22
MgO	23.61	7.06	17.22	9.83	14.53	8.62	6.90 (0.11)	6.13	6.61
CaO	9.15	11.79	11.14	10.40	11.60	11.38	12.40 (0.20)	11.15	10.18
Na ₂ O	0.81	2.61	1.22	2.36	1.78	2.37	2.37 (0.15)	2.37	2.37
K ₂ O	0.03	0.17	0.04	0.06	0.13	0.25	0.26* (0.03)	0.28	0.56
P ₂ O ₅	0.00	0.03	0.02	0.00	0.08	0.10	0.15* (0.05)	0.09	0.22
Total	98.22	98.84	99.49	98.46	99.72	98.98	100.15	99.73	98.48
Mg/(Mg + Fe)	0.748	0.636	0.705	0.648	0.701	0.614	0.481	0.446	0.480

The ratio of molecular Mg/(Mg + Fe) is to use total iron.

The calculated parental composition represents an average for six liquid lines of descent being intersected at 1165°C (Fig. 11).

Concentrations of K₂O and P₂O₅ for the calculated melt correspond to an average for three samples with higher contents of these elements (EG4507, UT-08, KT-47).

The experimental composition represents a glass after melting the cumulate EC-22 at QFM buffer (Hoover, 1989).

(Frenkel et al., 1988b). It is noteworthy that this technique can be applied also to large compositional datasets, even if it is difficult to make suggestions concerning primary cumulus assemblages. In that case, the problem of the identification of one or several parental melt compositions could be solved statistically, by finding the most compact clusters including both major and trace element contents (Frenkel et al., 1988a).

3.4.2. Geochemical Thermometry of the Skaergaard marginal cumulates

To reconstruct scenarios of the Skaergaard magma evolution at the earliest stages, just after its emplacement, we applied the Geochemical Thermometry technique to six widely contrasted rocks (Table 5). All these samples represent cumulus rocks from the Marginal Border Series: five were selected within 1 to 8.5 m from the intrusive contact (Hoover, 1989), whereas the EG4507 composition was supposed to resemble 'the chilled marginal gabbro' firstly used as a parental Skaergaard magma (Wager and Brown, 1967). These contact rocks represent almost ideal compositions to which to apply Geochemical Thermometry, mostly because they have no any clear record of magma (parental melt) fractionation. Another reason to use this computational technique is the contrasting compositions of the selected rocks, varying from high-Mg olivine-rich to high-Al plagioclase-rich cumulates (Table 5). This is important. For in our experience of the application of Geochemical Thermometry to different compositions, the more contrasted the compositions used, the more accurate are the estimates of the trapped (parental) liquid temperature and composition (Barmina et al., 1989a,b; Chalokwu et al., 1993).

Using compositions of these six rocks as starting liquids, the course of equilibrium crystallization up to a total crystallinity of 80% was calculated with the COMAGMAT-3.5 model. These calculations were conducted at 1 atm pressure, under dry conditions and the QFM buffer, with the crystal increment $\Delta\varphi_{cr} = 1 \text{ mol}\%$.

3.4.2.1. Crystallization sequences. The calculated appearance of minerals on the liquidus corresponds well to the initial compositions, with a wide high temperature field of olivine for high-magnesia sam-

ples (UT-04, EC-10, KT-47) and an early crystallization of plagioclase for UT-08 (Table 5):

UT – 04: Ol(1443°C) → Aug(1233°C)
→ Pl(1174°C),

UT – 08: Pl(1332°C) → Ol(1231°C)
→ Aug(1164°C),

EC – 10: Ol(1385°C) → Aug(1199°C)
→ Pl(1187°C),

MEO – 18: Pl + Ol(1248°C) → Aug(1161°C),

KT – 47: Ol(1346°C) → Pl(1191°C)
→ Aug(1189°C),

EG4507: Pl(1242°C) → Ol(1225°C)
→ Aug(1163°C).

Two samples, MEO-18 and EG4507, indicate sub-cotectic phase relations (Pl + Ol) in the range 1230–1250°C. It is important also that in four cases when Aug was calculated to be the third crystallizing mineral, these temperatures were no less than 1161°C. Petrological observations also provide evidence that high-Ca clinopyroxene in the Skaergaard intrusion was the third crystallizing mineral in the Layered Series, appearing soon after crystallizing a small amount on the Ol + Pl cotectic (Wager and Brown, 1967; McBirney, 1989, 1996). Thus the calculated temperature of about 1160°C should be considered a lower limit for the trapped liquid temperature we are looking for.

3.4.2.2. Liquid lines of descent. Modeled trajectories of the probable trapped liquid evolution are shown in Fig. 11. In the temperature–composition coordinates these lines look like a 'wisp' demonstrating a closing together followed with an obvious intersection at the range of 1175–1155°C. This intersection of the equilibrium lines is consistent with the premise that the selected cumulates are really mechanical mixtures of cumulus crystals plus a trapped (parental) melt, otherwise the liquid lines of descent for several various samples would not intersect (Frenkel et al., 1988a).

Visually, the temperature of this intersection corresponds to about $1165 \pm 10^\circ\text{C}$ —the value could be accepted as the primary equilibrium temperature at which a trapped (probably parental) melt was cap-

tured by these cumulates (Fig. 11). Average liquid composition representing this cluster of six evolutionary lines is given in Table 5. Also present here is an experimental liquid composition obtained at 1160°C after melting of another marginal cumulate EC-22 (Hoover, 1989). Comparison of the calculated and experimentally obtained trapped liquids indicates the close similarity of these compositions, with the exception of the CaO content which is overestimated by about 1 wt.% in the COMAGMAT simulations (Fig. 11). From the other side, the differences between these estimated trapped liquids are less than the differences with respect to the chilled margin gabbro KT-39, which is relatively enriched with incompatible components, such as TiO₂, K₂O, and P₂O₅ (Table 5).

At this stage, it is difficult to say unambiguously if the observed differences are within the uncertainties of experimental, computational, and analytical techniques, or due to some principal differences in the cooling history of the marginal cumulates. In any case, these data indicate that an enlarged spectrum of possible parental melt compositions should be included in the considerations concerning the differentiation of the Skaergaard magma. Coming back to the problem of trapped liquid compositions obtained experimentally by McBirney and Naslund (1990), we conclude that those represent not primary, but relatively low temperature residual melts. Similar iron and titanium enriched compositions were also obtained in the COMAGMAT calculations simulating the course of equilibrium crystallization at the temperatures < 1150°C (Fig. 11).

3.5. Simulating fractionation of the Skaergaard parental melts

A new version of the COMAGMAT-3.5 model was used to quantify the effect of the redox conditions on the fractionation of two proposed Skaergaard parental melt compositions. The first one corresponds to an average trapped melt composition TM calculated from the modeled (1165°C) and experimental (1160°C) liquids (Table 5); KT-39 is the second selected parental melt (Hoover, 1989). Simulations of the course of fractional crystallization were carried out at 1 atm pressure, with the crystal increment $\Delta\varphi_{cr} = 1$ mol%, up to the crystallinity of 80

mol%. Redox conditions of these calculations are given representing crystallization under the QFM and WM oxygen buffers.

3.5.1. The crystallization sequences

Fig. 12 illustrates the mineral crystallization sequences of the simulated fractionation. As shown in these plots, the calculated liquidus temperatures for TM are of 1158°C for QFM and 1163°C for WM buffer; in the case of KT-39 these temperatures are 1170°C and 1174°C, respectively. For the TM parent, the modeled crystallization sequence is Ol + Pl + Aug → Pl + Aug + Mt which is independent of the redox conditions. The main differences between calculations at QFM and WM buffers, lies in the higher crystallization temperature for Mt at more oxidizing conditions (Fig. 12).

For the KT-39 composition, calculated phase relations turned out to be more complex. The modeled crystallization sequence for silicate minerals is also independent of f_{O_2} , whereas for the appearance of iron–titanium oxides at the liquidus displays small, yet significant differences: Ol → Ol + Pl → Ol + Pl + Aug → Pl + Aug + Mt → Pl + Aug + Mt + Ilm (at QFM); and Ol → Ol + Pl → Ol + Pl + Aug → Pl + Aug + Ilm → Pl + Aug + Mt + Ilm (at WM). The calculated sequence at QFM within the 10–15°C COMAGMAT accuracy level is well correlated with experimental data obtained on the KT-39 composition (Hoover, 1989). The variance in the onset crystallization temperatures for ilmenite and Ti-magnetite at QFM and WM is in good agreement with the experimental data by Toplis and Carroll (1995).

3.5.2. Evolution of mineral compositions

Changes in the compositions of the modeled minerals are also displayed in Fig. 12. The most magnesian Ol was calculated to contain 74–76% Fo, whereas the initial Pl composition is uniform, with 62–63 mol% An. This is in a marked disagreement with experimental data by Hoover (1989), who obtained liquidus plagioclase at 1170°C to contain 73% An for KT-39. It is interesting, however, that Hoover himself indicates that there were observed no compositions more basic than An₆₂ among the cores of natural plagioclases in the KT-39 sample. The calculated high-Ca pyroxene compositions were varied in the range En₄₄Wo₄₁ near the liquidus to En₂₆Wo₃₀ at

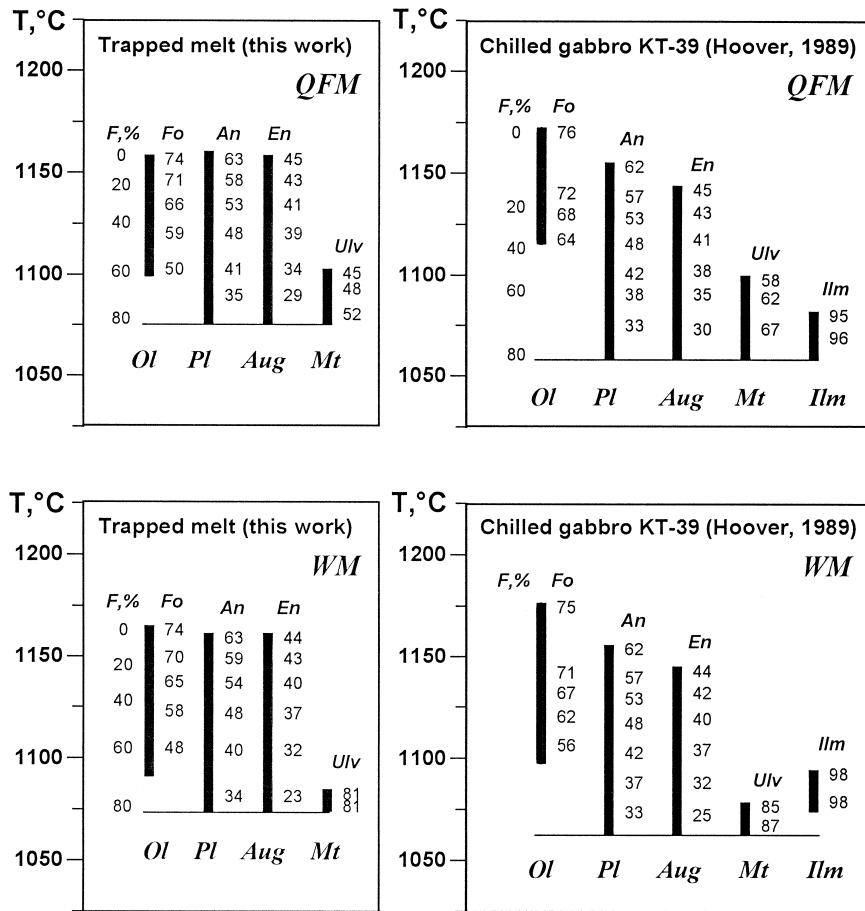


Fig. 12. Mineral crystallization sequences modeled at the fractionation of an average trapped melt (TM) and chilled gabbro (KT-39). Simulations were conducted with the COMAGMAT-3.5 model at 1 atm and QFM to WM oxygen buffer conditions. Values to the right of magnetite and ilmenite lines represent the percent of ulvöspinel and ilmenite component in solid solutions calculated using the equations of Stormer (1983).

the late stage. The amount of ulvöspinel (Ulv) and ilmenite components in the Fe–Ti oxide solid solutions was calculated using the equations of Stormer (1983). Compositions of Mt and Ilm in Fig. 12 are well correlated with changes in the oxidizing conditions.

3.5.3. Liquid lines of descent

Fig. 13 shows the evolution of FeO_{tot} and SiO_2 contents in the residual melts calculated as the fractionation products of TM and KT-39 at QFM conditions. Each of the compositions is represented by two evolutionary lines: the upper one includes calculations without any temperature corrections in CO-

MAGMAT-3.5, whereas the lower line represents a corrected model. Those corrections include slightly decreased modeled temperatures for Ol, Pl, and Aug (-10°C), and increased temperatures for Mt and Ilm ($+15^\circ\text{C}$). The given shift in the modeled temperatures corresponds to the above discussed accuracy of the COMAGMAT model (see Section 2), providing a maximal estimate of possible shift for the calculated evolutionary lines.

As follows from this plot, the summarized shift in the calculated temperatures of 25°C results in the changes of the maximal degree of FeO_{tot} enrichment to be 1.5–2.5 wt.% at the same SiO_2 content. This is comparable with the effect of oxygen fugacity on the

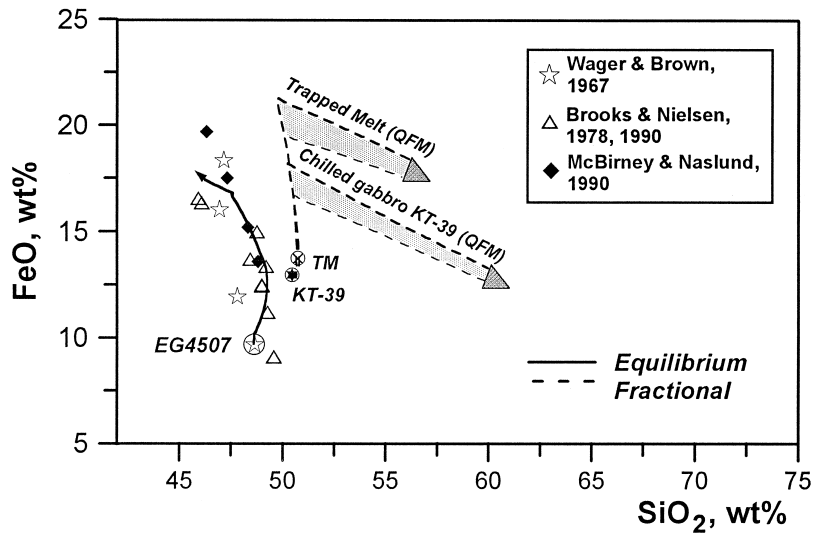


Fig. 13. Calculated and natural differentiation trends proposed to the Skaergaard intrusion. Liquid lines of descent for TM and KT-39 compositions represent calculated fractional crystallization products at 1 atm and QFM conditions. For each of the compositions two modeled lines are presented, covering the range of uncertainties of the COMAGMAT-3.5 model (see text). The evolutionary line to the left of the fractionation curves belongs to the simulations of equilibrium crystallization for the previously discussed chilled gabbro EG4507 (Wager and Brown, 1967). Filled diamonds correspond to trapped melts obtained in the melting experiments with cumulates from the Lower and Middle Layered Series (McBirney and Nakamura, 1974; McBirney and Naslund, 1990). Open triangles include dike rock compositions which were suggested to resemble the Skaergaard differentiation trend (Brooks and Nielsen, 1978, 1990).

onset of magnetite crystallization within 0.5–1.0 log f_{O_2} units. This is an important note, because the calculated phase equilibria information shown in Fig. 12 permits one to suggest small but well defined variations in f_{O_2} conditions. Accounting for the uncertainties of the COMAGMAT model, the following conclusions could be drawn from the results of modeling fractional crystallization (Fig. 13):

(1) Both calculated liquid lines of descent exhibit only minor decreases in SiO_2 contents in the melt, as compared to the proposed Skaergaard FeO– SiO_2 trend (Wager and Brown, 1967; Brooks and Nielsen, 1978, 1990; McBirney and Naslund, 1990).

(2) Both trajectories indicate a determined inflection point, where the content of SiO_2 starts to increase due to the appearance of Mt in the crystallization sequence.

(3) The TiO_2 enriched KT-39 composition (Table 5) demonstrates a less pronounced effect on iron enrichment, with a systematic difference of 2.5–3 wt.% FeO_{tot} between the TM and KT-39 trajectories—Fig. 13.

(4) The maximum possible extent of iron enrichment in the parental melts can reach 20–23 wt.% FeO_{tot} .

3.6. Significance of the modeling for the Skaergaard magma differentiation problem

Results of comparisons of the modeled and natural trends (Fig. 13) leave two main alternatives in solving this problem. This first one has already been discussed in the previous sections and includes the hypothesis that the Skaergaard magma gives an example of a common evolution of ferro-basaltic magmas, such as observed in volcanic environments (Hunter and Sparks, 1987, 1990), with some differences related to closed system crystallization (Toplis and Carroll, 1996). This interpretation implies that the classic trend of Wager and Brown (1967) may be flawed by erroneous relative volumes of the Skaergaard zones, mostly due to the venting of a significant amount of silicic differentiates (Hunter and Sparks, 1987, 1990; Ariskin et al., 1988; Toplis and Carroll, 1996).

Another explanation may be based on the premise that *the parental Skaergaard magma never was a pure liquid or a melt with a small amount of suspended crystals*. In such case, neither of the proposed parental melts (TM and KT-39) represent the parental Skaergaard magma, with the calculated perfect fractionation trends in Fig. 13 not resembling a real crystal fractionation process which occurred in the Skaergaard magma chamber. One can expect, if the Skaergaard magma came to the chamber with a significant amount of crystalline material, its liquid evolution would be in some way intermediate between equilibrium and fractional crystallization of the crystal saturated magma.

To support this hypothesis, an additional calculated liquid line of descent is shown in Fig. 13. It belongs to the simulations of equilibrium crystallization for the previously discussed chilled gabbro EG4507 (Wager and Brown, 1967). One can see that the modeled line much better fits the silica depletion trend, including both experimental data by McBirney and Naslund (1990) and dike rock compositions of Brooks and Nielsen (1978, 1990). This coincidence does not mean that the Skaergaard intrusion was completely solidified by the equilibrium crystallization mechanism. It may only indicate a serious petrogenetic role of residual melts with compositions controlled by a large amount of equilibrium suspended or accumulated mineral phases.

3.6.1. Geological interpretation of Geochemical Thermometry results

The second hypothesis based on the assumption of a large amount of equilibrium minerals allows us to formulate some geological and petrogenetic conclusions. One can suggest that the trapped parental melts and in situ derivative residual melts might migrate upward from the Lower and Middle Zones of the Skaergaard intrusion, as a result of compaction of the lower cumulates (Naslund and McBirney, 1996; Boudreau and McBirney, 1997). This could change their compositions by the magmatic metasomatism mechanism (Irvine, 1980), with chemical sequences being opposite to that followed from simple fractional crystallization (Frenkel et al., 1988b). This common fractionation process operating through settling of crystals inward from the roof was probably limited by the upper parts of the magma cham-

ber, where the amount of crystals suspended in the magma was much less than in the lower zones. This situation could explain the small amount of siliceous differentiates relative to the total volume of the Skaergaard magma chamber.

Results of Geochemical Thermometry indicate EG4507 to contain at least 45 wt.% of OI and PI at the estimated emplacement temperature of 1165°C (Fig. 11). In this context, petrologists again should draw more attention to the ‘cumulus’ chilled marginal gabbro similar to the EG4507 composition, as a composition resembling the parental Skaergaard magma (Wager and Brown, 1967). It contains OI and PI in close to cotectic relations and during equilibrium crystallization exhibits an evolutionary trend similar to that followed from natural and experimental observations (Fig. 13). It is important that the evidence for the proposed complex fractionation hypothesis is similar to the mass balance constraints used by Wager and Brown (1967) and Hunter and Sparks (1987), and it would be erroneous to apply this technique to the whole magma body.

Note once more, this combined fractionation, including in situ crystallization and residual melt migration in the lower zones paired with the crystal settling in the upper part, does not contradict that the TM and KT-39 compositions present correctly estimated trapped/parental liquids. The proposed two layer structure of the Skaergaard magma chamber assumes different regimes of chemical evolution of the parental melts which could not fractionate by an efficient separation of minerals within an initially highly crystallized lower part of the magmatic system. Probably, a systematic Geochemical Thermometry of the Skaergaard intrusion rocks, both vertically and in parallel to the magmatic layering, would provide more insight into the evolution of the melt compositions in different parts of this intrusion.

To conclude this section, I would suggest that the classic Wager’s trend inferred from the structure of the Skaergaard intrusion should be considered as an exception rather than a rule for the differentiation of ferro-basaltic magmas. This trend is probably peculiar to the residual melts separated from highly crystallized systems, which may have been fractionated under closed (with respect to oxygen) conditions (Toplis and Carroll, 1996). Magmas of same ferro-basalt composition containing small amounts of sus-

pended crystals will fractionate with the formation of differentiates similar to the TM and KT-39 trends shown in Fig. 13.

4. Simulating polybaric fractionation of high-magnesia magmas and the formation of high-alumina basalts from Klyuchevskoi volcano, Kamchatka

In this section we will consider another example of magma fractionation in a volcanic system generating parental magmas essentially free of suspended crystals, mostly due to an efficient separation of mafic minerals at depth. The purpose of this study is to present a quantitative genetic interpretation of the magmatic series of Klyuchevskoi volcano (Eastern Kamchatka, Russia). The lavas characteristic of this volcanic centre range from high-Mg basalts (HMB) to high-Al basalts (HAB). To identify the petrological processes responsible for the observed suite of basalts, we used the COMAGMAT model to simulate the formation of the Klyuchevskoi suite assuming isobaric crystallization of a parental HMB magma at a variety of pressures (1 atm, 2.4, . . . 20 kbar), and a separate set of simulations assuming fractionation during continuous magma ascent from a depth of 60 km. The model that produced the best fit to the magmatic series indicates that the petrochemical trend can be produced by ~40% fractionation of observed Ol–Aug–Sp ± Opx assemblages during ascent of the parental HMB magma over the pressure range 19–7 kbar at 1350–1110°C, with ~2 wt.% of H₂O in the initial melt and ~3 wt.% of H₂O in the resultant high-Al basalt (Ariskin et al., 1995). The decompression hypothesis is in good agreement with seismic data suggesting the absence of a magma chamber under Klyuchevskoi volcano, where an isobaric fractionation process could proceed (Fedotov et al., 1990; Ozerov et al., 1997). This polybaric mechanism is suggested to be typical for large island-arc volcanic centres with a deep-seated feeding system integrated into magma-generating zones in the upper mantle.

4.1. Origin of island-arc high-alumina basalt

Hypotheses regarding the generation of subduction related high-Al basaltic magmas can be divided

into two main groups. The first one rose from the classic work by Kuno (1960) who believed HAB to be a primary magma generated by the partial melting of a mantle peridotite. Later, this idea of a primary HAB magma was transformed to another hypothesis that high-Al basalts represent partial melts of subducted oceanic crust, including the incorporation of sedimentary material in the melting zones (Babansky et al., 1983; Baker and Eggler, 1983; Brophy and Marsh, 1986; Johnston, 1986). This view is based mostly on the results of phase equilibria experiments with HAB which have high-pressure anhydrous liquids defined by garnet and clinopyroxene (Baker and Eggler, 1983; Johnston, 1986), see also the review by Myers and Johnston (1996).

An alternative group of hypotheses was proposed to consider high-Al basalts as derivative magmas characterized by the enrichment with Al₂O₃ caused by a delay in the plagioclase crystallization from hydrous picrite–basalt magmas (Yoder and Tilley, 1962). These magmas are supposed to be mantle-derived high-magnesian melts which could fractionate at moderate to low pressure to produce HAB liquids (Perfit et al., 1980; Kay and Kay, 1985; Nye and Reid, 1986; Uto, 1986; Kersting and Arculus, 1994). This hypothesis was partly supported by a series of anhydrous experiments with high-Mg basalts at 1 atm to 20 kbar pressure (Gust and Perfit, 1987; Kadik et al., 1990; Draper and Johnston, 1992). Experimental glasses produced at the pressures above 8 kbar were found to contain 16–18 wt.% Al₂O₃, thus approximating, in general, the natural HAB, with the exception of CaO contents and alkalis (see the discussion below). The observed differences might be ascribed to the absence of water in the above experiments. Unfortunately, the number of hydrous experiments with HMB is not sufficient to support this view unambiguously (Tatsumi, 1982; Tatsumi et al., 1983; Sisson and Grove, 1993a,b).

Other approaches to the interpretation of high-Al basalts include the mechanical accumulation of plagioclase crystals circulating in less aluminous magmas (Crawford et al., 1987; Plank and Langmuir, 1988; Brophy, 1988; Fournelle and Marsh, 1991), as well as the reaction of ascending magmas with mantle wallrock (e.g., Kelemen, 1990). This wide spectrum of proposed hypotheses allows one to suggest that HAB may be produced in a variety of ways,

even by a combination of different mechanisms. Nevertheless, it is undoubtedly true that the main focus of the origin of high-Al basalts is whether the igneous rocks represent primary or non-primary magmas, see reviews by Crawford et al. (1987) and Kadik et al. (1990).

In this context, geological observations indicating that high-alumina basalts are often associated with

high-magnesia basalts are of great importance. Such associations have been observed at the Okmok and Makushin volcanoes in the Aleutian Islands (Nye and Reid, 1986; Gust and Perfit, 1987) and at the Klyuchevskoi volcano in Kamchatka (Khrenov et al., 1990; Kersting and Arculus, 1994). Despite their relative scarcity, HMB drew attention as potential parental magmas derived from the upper mantle. The

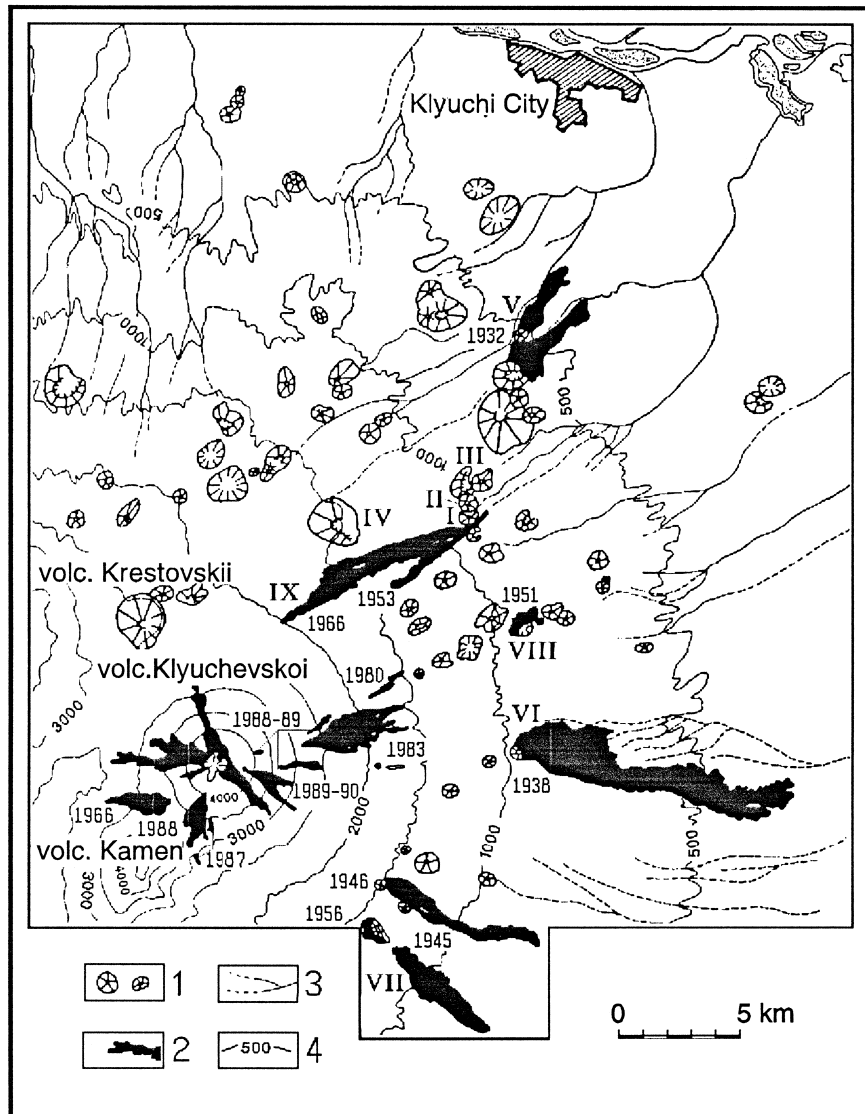


Fig. 14. Location map of Klyuchevskoi volcano boccas, modified after V.N. Dvigalo (Institute of Volcanology). (1) Cinder cones (I—Bulochka, II—Novograbenov, III—Luchitskii, IV—Slyunin); (2) 1932–1990 lava flows and the years of eruptions (V—Tuila, VI—Bilyukai, VII—Zavaritskii, VIII—Bylinkina, IX—Piip); (3) dry river beds; (4) contour lines.

main signature of its deep origin is a high magnesium number for Ol and coexisting pyroxenes which can reach 90–92% (Kay and Kay, 1985; Ariskin et al., 1995). It is interesting that such rare high-Mg minerals were also observed in HAB (Ozerov et al., 1996): this may be considered indirect evidence for the genetic link between HAB and HMB. High-magnesian compositions of melt inclusions observed in olivines (Fo_{87-90}) from Klyuchevskoi volcano support the proposed genetic relations (Sobolev and Chaussidon, 1996).

4.2. Petrology of Klyuchevskoi basalts

4.2.1. Geological setting of the Klyuchevskoi volcano

Klyuchevskoi volcano, the largest and most active volcanic centre in the Kamchatka peninsula, is located at the junction between the Kurile–Kamchatkan and Aleutian Island arcs. It was constructed on the slope of the older Kamen volcano, has a height of approximately 4800 m, and is about 7000 years old. This volcanic centre has a volume of 250 km^3 with a mean rate of magma discharge of 55 million tons per year (Fedotov et al., 1990). The volcanic edifice consists of numerous basalt lava sheets and

pyroclastic materials, ranging continuously from high-Mg basalts with $> 10\%$ MgO, to high-Al basalts with $> 18\%$ Al_2O_3 (Khrenov et al., 1990; Kersting and Arculus, 1994; Ariskin et al., 1995). The cone of the Klyuchevskoi volcano is built up of 90% aluminous basalts, the remaining 10% are magnesian and intermediate varieties (Khrenov et al., 1990).

Records of its eruptive activity from the 18th century to 1932 indicate merely eruptions from the summit crater. Because those were mostly explosive and, occasionally, explosive–effusive events, the volume of pyroclastic material in the cone is substantially larger than that of lava flows. In 1932, a drastic change in the Klyuchevskoi volcano activity was observed: along with continued eruptions from the central crater, flank eruptions began to take place, commonly once every 4 years (Fedotov et al., 1990). Sixteen large flank eruptions have occurred since 1932 with the formation of extensive lava flows, ranging between hundreds of meters to 7 to 8 km in length. These flank eruptions usually proceeded from several radial fissures located mostly on the north-eastern, eastern, and southeastern slopes. In addition, there are more than 100 cinder cones on the slopes of the Klyuchevskoi volcano (Fig. 14).

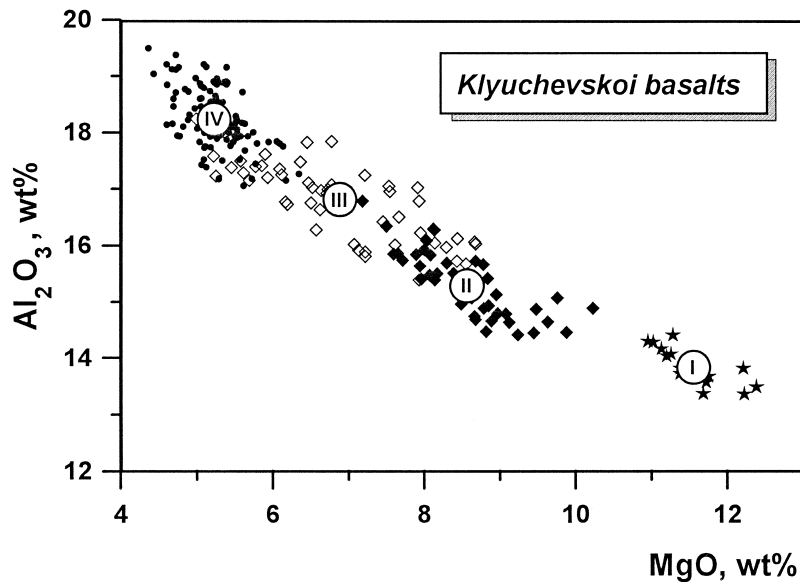


Fig. 15. Variation diagram for Klyuchevskoi basalts. I, II, III and IV correspond to average compositions of four types listed in Table 6.

4.2.2. Classification of Klyuchevskoi basalts

Earlier, the Klyuchevskoi lavas have been divided into two groups—*magnesian* and *aluminous* basalts, with transitional varieties assumed to contain about 7 wt.% MgO and 16–17 wt.% Al₂O₃ (Khrenov et al., 1990). The two-member division of the Klyuchevskoi basalts was based on the use of MgO–Al₂O₃ diagrams (Fig. 15) making it difficult to compare these rocks with other magma types from subduction zone volcanoes. To avoid a terminological confusion, we have processed 242 compositions of Klyuchevskoi basalts using a sophisticated classification program called PETROTYPE (Ariskin et al., 1995). It allows us to divide the whole set of analyses into four groups: high-magnesia (15 samples), magnesian (46), aluminous (50), and high-*alumina* (131) basalts—Table 6.

The observed changes, from high-magnesia to high-alumina basalt, are marked by a monotonous increase in the SiO₂, TiO₂, Al₂O₃, Na₂O, K₂O, and

P₂O₅ contents, with a complementary decrease in MgO and CaO. The content of FeO remains approximately constant, therefore, the MGN = Mg/(Mg + Fe) value declines from approximately 0.7 to 0.5 in more aluminous rocks (Table 6). These features provide evidence for fractionation of a primary high-Mg magma through the separation of mafic minerals (with or without insignificant plagioclase crystallization) which may have been a process that controlled the formation of the Klyuchevskoi series. This suggestion is correlated with the evolution of normative compositions in Table 6, which demonstrates a marked decrease in the contents of olivine and diopside from group I to group IV. It led us to conclude that the fractionation of Ol and high-Ca Cpx may have played a dominant role in the formation of chemical diversity of the magmatic series. This conclusion is supported by the compositional evolution of phenocrysts and mineral inclusions observed in the Klyuchevskoi basalts.

Table 6
Chemical and normative composition of main types of Klyuchevskoi basalts (Ariskin et al., 1995)

Type <i>n</i>	High-Mg basalt (I) 15	Magnesian basalt (II) 46	Aluminous basalt (III) 50	High-Al basalt (IV) 131
<i>Component</i>				
SiO ₂	51.76 (0.34)	53.39 (0.55)	53.22 (0.78)	53.50 (0.48)
TiO ₂	0.86 (0.07)	0.84 (0.11)	0.95 (0.13)	1.09 (0.07)
Al ₂ O ₃	13.86 (0.33)	15.29 (0.55)	16.79 (0.66)	18.26 (0.50)
FeO _{tot}	8.83 (0.18)	8.52 (0.24)	8.83 (0.47)	8.67 (0.33)
MnO	0.17 (0.01)	0.17 (0.02)	0.17 (0.04)	0.16 (0.02)
MgO	11.55 (0.43)	8.58 (0.65)	6.89 (1.00)	5.24 (0.34)
CaO	9.73 (0.20)	9.41 (0.30)	8.91 (0.46)	8.22 (0.38)
Na ₂ O	2.47 (0.18)	2.72 (0.24)	3.11 (0.32)	3.45 (0.20)
K ₂ O	0.63 (0.09)	0.90 (0.15)	0.96 (0.19)	1.20 (0.10)
P ₂ O ₅	0.15 (0.02)	0.18 (0.03)	0.18 (0.04)	0.20 (0.04)
Mg/(Mg + Fe)	0.699	0.641	0.580	0.517
Ca/(Ca + Al)	0.561	0.528	0.491	0.450
<i>CIPW, wt.%</i>				
Or	3.72	5.32	5.67	7.09
Ab	20.90	23.01	26.31	29.19
An	24.88	26.86	29.02	30.80
Di	18.18	15.24	11.54	7.20
Hy	17.93	25.04	21.96	21.15
Ol	12.42	2.52	3.28	2.02
Ilm	1.63	1.60	1.80	2.07
Ap	0.36	0.43	0.43	0.47

Compositions were normalized to 100 wt.%.

Standard deviations for each composition (1σ) are given in parentheses.

4.2.3. Mineralogy of Klyuchevskoi basalts

4.2.3.1. Petrographic description. The Klyuchevskoi lava's are vesicular or massive basalts containing abundant phenocrysts of olivine and high-Ca clinopyroxene (augite). Occasional grains of plagioclase may be observed in the magnesian basalts, but systematic occurrence of the mineral phenocrysts is commonly recorded in the aluminous to high-alumina varieties. These phenocrysts range between 0.1 and 1 mm in size; rare grains of olivine and pyroxene can reach 5–7 mm across. All of the rock types contain abundant glomerocrysts, which may be as large as 10 mm. The Ol–Cpx assemblage is dominated by olivine in highmagnesia basalts and by clinopyroxene in the magnesian and aluminous basalts. Occasional orthopyroxene grains, sometimes interlocked with plagioclase or clinopyroxene, have been found only in the aluminous and high-alumina basalts. However, during microprobe studies Opx was identified as solid-phase inclusions in both Ol and Cpx in all rock types (Ozerov et al., 1996). Cr-rich spinel (picotite) occurs as inclusions in olivines, especially from the high-magnesia and magnesian basalts. The total amount of phenocrysts and glomerocrysts varies between 3 and 7 vol.% in the high-magnesia and magnesian rocks and may reach as high as 20 vol.% in the high-alumina basalts. The groundmass varies from vitrophyric to intersertal. It is dominated by thin plagioclase laths and fine intergrowths of olivine, clinopyroxene (augite or pigeonite), and titanomagnetite. The mesostasis consists of slightly altered or devitrified glass, which has an andesite–dacite composition in the aluminous basalts (Ozerov et al., 1996).

4.2.3.2. Microprobe studies. Chemistry of rock-forming minerals from the Klyuchevskoi lavas has been reported in a series of papers published in the Russian literature by Ozerov and Khubunaya (Institute of Volcanology, Petropavlovsk–Kamchatskii, Russia). More recent data include publications by Kersting and Arculus (1994), Ariskin et al. (1995), and Ozerov et al. (1996). These compositional data reveal several points of present interest.

First, there is a fairly magnesian assemblage of Cpx (MGN = 87–90) and Ol (MGN = 88–92), which contain numerous inclusions of Cr-, Al-, and

Mg-rich spinel with occasional orthopyroxene (up to MGN = 89). Such high-Mg minerals are most abundant in the high-magnesia and magnesian basalts, however, they also may occur in the aluminous and high-alumina rocks. Second, the compositions of the cores of Ol, Cpx, and Opx in the phenocrysts and mineral inclusions indicate considerable variations, ranging from MGN of 90 to MGN = 65–70 in the same sample. Third, the composition of Pl phenocrysts varies from An_{84–85} to An₆₀, however, the MGN number of Ol and pyroxene inclusions in the plagioclase never exceeds 72–76 (Ozerov et al., 1996). This indicates Pl to be a late mineral phase in the Klyuchevskoi magma crystallization sequence.

Many of Ol and Cpx phenocrysts exhibit normal zoning manifested in the more ferroan outer zones, with the compositional differences not exceeding a few mol%. Some samples demonstrate a more complex zoning, from normal to reversed and vice versa, which is particularly distinct in the clinopyroxene grains (Kersting and Arculus, 1994). This pattern is interpreted as an indication of magma compositional heterogeneity produced by the mixing of liquid fractionation products prior to the eruptive phase (Sakuyama, 1981). The distinct bimodal distribution of the mineral compositions in the most of Klyuchevskoi lavas is supportive of mixing (Ozerov et al., 1996).

4.2.4. Petrogenetic significance of Ol–Cpx–Sp glomerocrysts

We conducted a detailed microprobe study of the mafic mineral compositions with the goal of defining the compositions of coexisting olivine and clinopyroxene glomerocrysts (Ariskin et al., 1995). About, 11 samples from 10 lava flows representing all types of the Klyuchevskoi basalts have been investigated. These analytical studies were carried out in the Microprobe Laboratory at Oregon State University (Corvallis, USA) using thin sections that have been scanned previously with an express probe to identify the polymineral intergrowths. The basic genetic assumption was that crystals constituting the glomerocrysts may represent cotectic assemblages that have been crystallized simultaneously from parental or derivative Klyuchevskoi magmas.

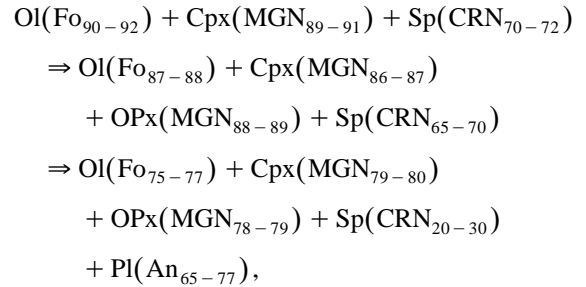
The observed relations between MGN values for clinopyroxenes and Fo contents in olivines are shown

in Fig. 16. Analyses of the coexisting minerals confirm that they represent an extremely magnesian association that can be correlated to the bulk rock type (Fig. 15). Interesting enough, the spinel inclusions in Ol also exhibit a fairly systematic decrease in Cr and Mg concentrations with the declining Fo content (Ariskin et al., 1995). This may imply that mafic magma fractionation controlled by the multiple saturated cotectic began early in the evolution of the Klyuchevskoi igneous system. The observed compositional relations for other mafic mineral pairs (Cpx–Opx and Opx–Ol) are similar to those shown in Fig. 16 (Ariskin et al., 1995; Ozerov et al., 1996). Thus, the results of microprobe studies of the coexisting (cotectic) mineral intergrowths and mutual mineral inclusions can be summarized as two principal conclusions on the origin of the Klyuchevskoi basalts:

(1) The broad range of mafic mineral compositions in the same sample indicates that, by the time of the eruption, these basalts represented radically non-equilibrium associations of the magmatic melt and suspended minerals. This allows one to suggest that both parental and derivative magmas (including

crystals produced during various stages of the magma fractionation) could be arbitrarily mixed in the Klyuchevskoi conduit.

(2) The range of compositions observed in the mineral pairs may be attributed to a set of related cotectic assemblages generated by progressive fractionation corresponding to the following sequence (Ariskin et al., 1995):



where $\text{MGN} = \text{Mg}/(\text{Mg} + \text{Fe}^{2+})$ and $\text{CRN} = \text{Cr}^{3+}/(\text{Cr}^{3+} + \text{Al}^{3+} + \text{Fe}^{3+})$. In order to put preliminary constraints on the initial conditions of this fractionation process, let us consider experimental data on Ol and Cpx compositions observed in 1 atm and high-pressure experiments.

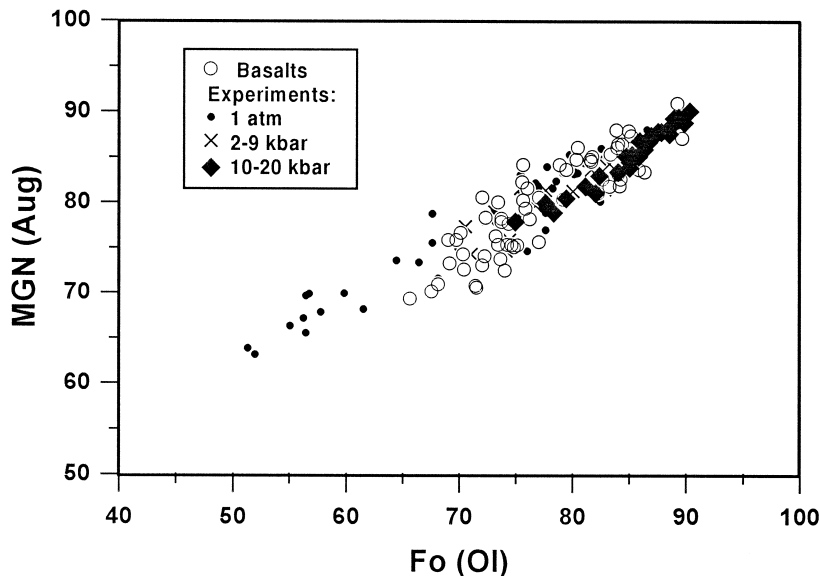


Fig. 16. Compositions of coexisting olivines and clinopyroxenes observed in Klyuchevskoi basalts and obtained in melting experiments. Natural compositions are from Ariskin et al. (1995). Experimental mineral compositions were extracted from the INFOREX-4.0 data base (Ariskin et al., 1997) and include results of 20 studies: 55 runs carried out at $P = 1$ atm and 44 runs in the range 2–20 kbar. This set of experiments represents runs with duration no less 12 h and glasses with $(\text{Na}_2\text{O} + \text{K}_2\text{O}) < 5$ wt.%.

These data have been extracted from the IN-FOREX database and also plotted in Fig. 16. This information represents the results of 20 studies including, 55 runs at $P = 1$ atm and 44 runs in the pressure range 2–20 kbar, for experimental glasses with $(\text{Na}_2\text{O} + \text{K}_2\text{O}) < 5$ wt.%. The distribution of these data as a function of pressure is of principal importance. As seen in Fig. 16, most of the experiments carried out at atmospheric pressure fall into the region of iron-rich compositions, reflecting the late crystallization of Cpx at the temperatures below 1180°C. At pressures of 2–9 kbar, the Cpx compositions overlap the MGN range of 74–85, whereas the most magnesian clinopyroxenes with MGN ~ 90 were obtained only in high-pressure experiments at $P = 15$ –20 kbar. These high-pressure Ol + Cpx assemblages were observed to be in equilibrium with highly magnesian experimental glasses, containing more than 10 wt.% MgO, similar to HMB of Klyuchevskoi volcano (Table 6). It allowed us to suggest that the average composition of high-magnesia basalts might be assumed to approximate magma parental to the volcanic suite, which probably began to crystallize at depths corresponding to pressures of 15–20 kbar (Ariskin et al., 1995).

4.3. Modeling the formation of high-alumina basalts of the Klyuchevskoi volcano

The proposed link between high-Mg basalts and HAB includes the removal of mafic phases, principally olivine and augite. Using the COMAGMAT-3.0 model (Ariskin et al., 1993), we have calculated Ol compositions on the liquidus of the average HMB (Table 6) for the pressure range of 0.001–20 kbar and oxygen fugacity corresponding to the QFM buffer. The calculated values fall into the range $\text{Fo}_{89.3-90.3}$ which is close to the most magnesian Ol compositions observed in the Klyuchevskoi lavas (Fig. 16). In order to conduct similar calculations for Cpx there is a need to specify a range of pressures at which Ol and Cpx may coexist on the liquidus. To approach the goal, a series of polybaric calculations simulating the course of equilibrium crystallization for the average high-Mg basalt at 1 atm to 20 kbar was carried out (Ariskin et al., 1995). The main results of these simulations are summarized in Figs. 17 and 18.

4.3.1. Simulating equilibrium crystallization of the Klyuchevskoi basalts at anhydrous conditions

The calculated anhydrous P – T phase relations of the average high-magnesia basalt are shown in Fig. 17 (see HMB plot). This phase diagram demonstrates common properties of basaltic systems concerning the expansion of the phase volume of pyroxene at the expense of Ol and Pl with increasing pressure. For further considerations it is important that at pressures of about 18 kbar, the high-Mg melt appears to be saturated with olivine ($\text{Fo}_{90.3}$) and augite (MGN = 89.8), that is, with the two main phases corresponding to the most magnesian mineral association observed in the Klyuchevskoi lavas (Fig. 16). This may be considered as one more indirect evidence for the high-pressure nature of the primary high-Mg association. The field of Opx (MGN = 89.7) is modeled to be close to the liquidus.

Two upper plots in Fig. 18 display a series of the liquid lines of descent calculated for the ‘dry’ polybaric conditions ranging from 1 atm to 20 kbar. The strong inflection in the CaO–MgO plot represents the point at which the magma encounters the Ol–Cpx cotectic. One can see that at pressures of more than 8 kbar equilibrium crystallization of the HMB composition results in Al_2O_3 -enriched liquids, which however, do not provide an adequate match with the range of natural compositions. The Klyuchevskoi trend appears to cross all the calculated lines, if the CaO–MgO diagram is used for comparisons (Fig. 18). This problem is somewhat similar to that encountered by Draper and Johnston (1992), who tried to apply results of high-pressure experiments with a high-magnesia basalt from Idak plateau for genetic interpretations of associated high-alumina basalts from Okmok volcano (Umnak Island, Aleutians). The lower-temperature experimental liquids were also poorer in CaO than typical HABs (see two lower plots in Fig. 18).

As noted by Johnston (1986) and Draper and Johnston (1992), this discrepancy could be resolved if there is a mechanism which permits olivine to be a liquidus phase for HAB at the appropriate pressure. However, Baker and Eggler (1983) and Johnston (1986) reported plagioclase as the liquidus phase up to ~ 17 kbar with clinopyroxene and garnet assuming the liquidus at progressively higher pressures under anhydrous conditions (see also the calculated

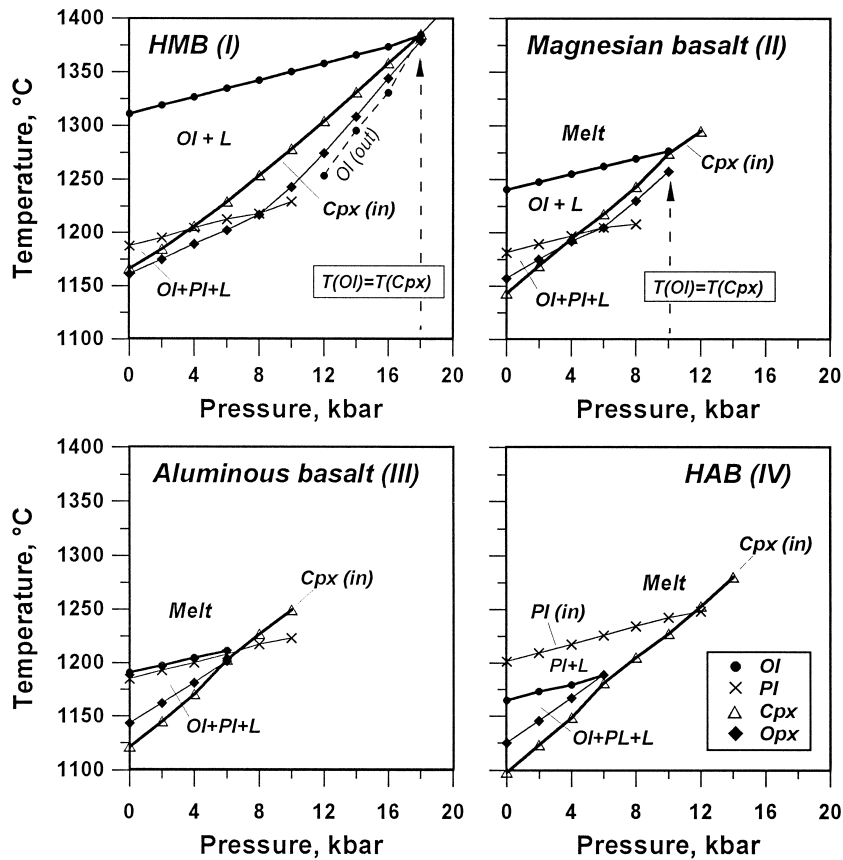


Fig. 17. Modeled anhydrous P - T phase relations of typical Klyuchevskoi basalts calculated with COMAGMAT-3.0 (Ariskin et al., 1993). The diagrams were constructed from isobaric equilibrium crystallization sequences calculated for four initial melts (see Table 6) at the pressures of 1 atm, 2, 4...20 kbar. These calculations were carried out with the crystallization increment $\Delta\varphi_{cr} = 1$ mol%, up to the total percent crystallized $\varphi_{cr}^{max} = 60\%$. The basic version of COMAGMAT-3.0 was slightly modified through small changes in 'high-pressure parameters' β for Aug and Opx (see Eq. (3)) in order to reduce the modeled field of Opx at high pressures, as it was assumed from natural observations.

P - T diagram for the average HAB of Klyuchevskoi volcano in Fig. 17). In an attempt to solve this problem, it was suggested that either (1) olivine is in a reaction relationship with HAB melts and so would not appear as a liquidus phase, or (2) water presence in the igneous system caused the primary crystallization of Ol to expand at the expense of Pl , so as to encompass HAB compositions (Draper and Johnston, 1992). Consideration of the results of melting experiments on HAB and HMB compositions indicates the Ol -melt reaction is unlikely to account for the lack of liquidus olivine in high-alumina basalts (Myers and Johnston, 1996). Thus, some amount of H_2O appears

to be necessary to enable high-Mg basalts to evolve to HAB through fractionation of mafic phases.

This suggestion is also true for the Klyuchevskoi basalts, but with one exception. Both mineralogical and petrochemical data provide evidence for the $Ol + Cpx$ cotectic controlling the formation of HAB at the entire range of compositions, from high-magnesia to Al_2O_3 enriched liquids: decreasing CaO contents in the natural series unambiguously indicates clinopyroxene was a cotectic phase with olivine (Fig. 18). However, at 8–18 kbar (i.e., in the range of modeled 'high-alumina basalt' compositions) there would be a large interval within which Ol would

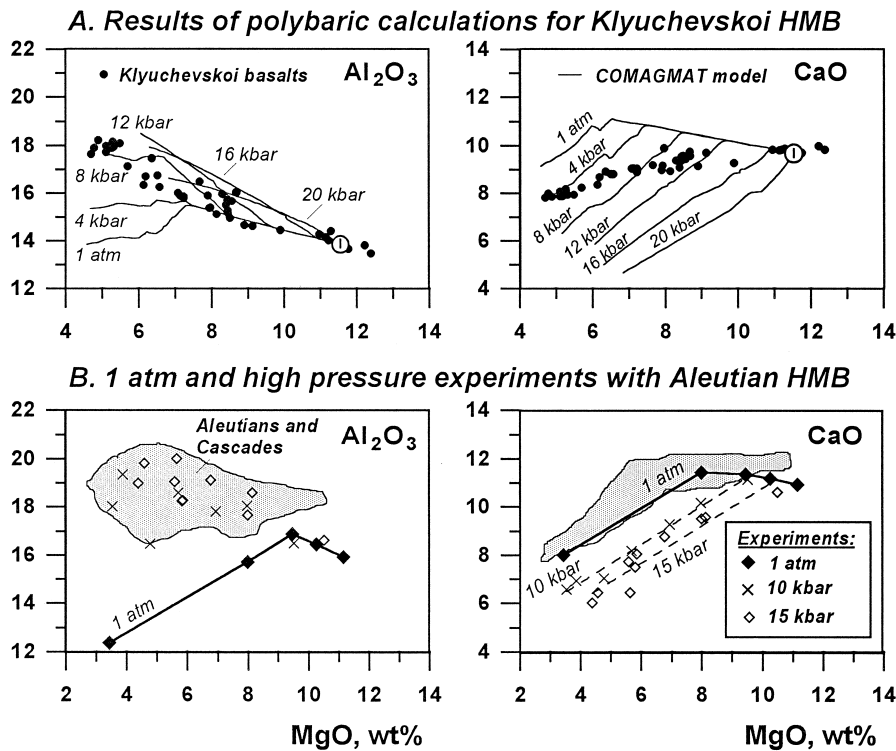


Fig. 18. Calculated and experimental liquid lines of descent for high magnesia basalts from Klyuchevskoi volcano (Kamchatka) and Okmok volcano (Aleutians). Calculations of equilibrium crystallization of the average Klyuchevskoi HMB were carried using a modified COMAGMAT-3.0 model (Ariskin et al., 1993). Representative compositions of the Klyuchevskoi basalts are from Ariskin et al. (1995). Experimental glass and natural HAB (Aleutians + Cascades) compositions are from Draper and Johnston (1992).

crystallize alone before Cpx would begin to form (Fig. 17, HMB plot). This would result in increasing CaO contents (see upper CaO–MgO diagram in Fig. 18). A possible explanation of these discrepancies is to link the formation of the observed suite with decompression fractionation of a parental high-magnesia magma containing a small but significant amount of water, during a continuous ascent from the depth of 60 km, corresponding to the calculated Ol + Cpx saturation point (Ariskin et al., 1995).

4.3.2. Simulating decompression fractionation of the Klyuchevskoi magma at water undersaturated conditions

If the series of Klyuchevskoi lavas was really produced by fractionation during decompression, then the more evolved basalts should be multiply saturated with Ol and Cpx at progressively lower pres-

ures. Results of phase equilibria calculations at anhydrous conditions for other types of Klyuchevskoi basalts do not contradict this decompression hypothesis. The average magnesian basalt is saturated with Ol and Cpx at 10–11 kbar, whereas aluminous basalt indicates the Ol + Pl + Cpx + Opx liquidus at ~7 kbar (Fig. 17). Moreover, the natural trends suggest that the proportion of high-Ca pyroxene crystallization at the Ol–Cpx–Sp cotectic was lower than that calculated assuming isobaric crystallization (Fig. 18). This fact could be also addressed to the decrease in the phase volume of clinopyroxene during decompression.

To constrain this hypothesis numerically, we have developed a subroutine of the COMAGMAT model to calculate changes in phase equilibria as the magma is assumed to simultaneously rise and fractionate (Ariskin et al., 1993). This subroutine was integrated into the COMAGMAT model as the *Decompression*

Crystallization routine (Fig. 1). This option allows the user to change the pressure during simulating the course of equilibrium or fractional crystallization by means of varying an input parameter called *the rate of decompression* $dP/d\varphi_{cr}$ (kbar/mol% crystallized).

On this basis a series of almost 600 forward models of the decompression fractional crystallization of the Klyuchevskoi HMB have been conducted. This series of calculations used different parameters, such as initial and final pressures of fractionation (from 18–20 kbar to 5–10 kbar), rate of decompression ($-0.50 \leq dP/d\varphi_{cr} \leq -0.10$), initial H_2O content in the parental magma (0.2–2.0 wt.%), as well the effect of water on mineral crystallization temperatures (Table 2). The purpose of this modeling was to constrain the conditions that would reproduce the natural trends. The model that produced the best fit to the observed suite of Klyuchevskoi lavas is shown in Figs. 19 and 20.

According to this optimal model, the proposed parental HMB magma, containing about 2 wt.% H_2O , began to fractionate with the Ol–Cpx \pm Sp cotectic at $P \sim 19$ kbar and $T \sim 1350^\circ C$. Olivine and augite fractionated with an average rate of decompression of $dP/d\varphi_{cr} = -0.33$ kbar/mol%, in the proportion $\sim 1:1.5$ up to $1260^\circ C$ (~ 15 kbar, $\varphi_{cr} = 15$ wt.%), when magnesian Opx (MGN = 87.8) joined the liquidus minerals. The continued fractionation of these minerals is distinguished by the increased amount of crystallizing Cpx (up to 90%). The proportion of Ol was decreased to 15–10 wt.% with that of orthopyroxene being as low as 2%. More efficient separation of Cpx resulted in the CaO–MgO trend bending toward a greater decline in CaO at the late stages of the polybaric crystallization (Fig. 19). Plagioclase was calculated to crystallize at a pressure of 7 kbar, a temperature of $1110^\circ C$, and about 3 wt.% H_2O in the residual melt. At this stage, the bulk degree of fractionation with respect to the initial

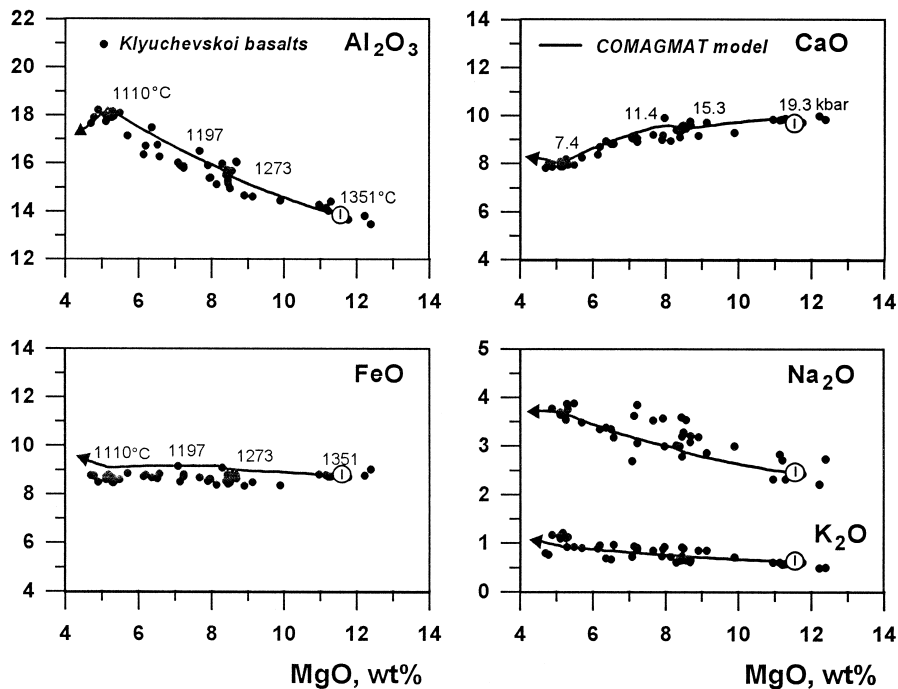


Fig. 19. Modeled trends of decompression fractional crystallization for the average Klyuchevskoi high-Mg basalt (Type I from Table 6). Calculations were carried using a modified COMAGMAT-3.0 model (Ariskin et al., 1993), assuming crystal increment of 1 mol%, initial pressure $P = 19.3$ kbar, the rate of decompression $dP/d\varphi_{cr} = -0.33$ (kbar/mol%), initial water content 2 wt.%, and QFM buffer (Ariskin et al., 1995). Values near the calculated lines represent decrease in the temperature and pressure during the decompression fractionation.

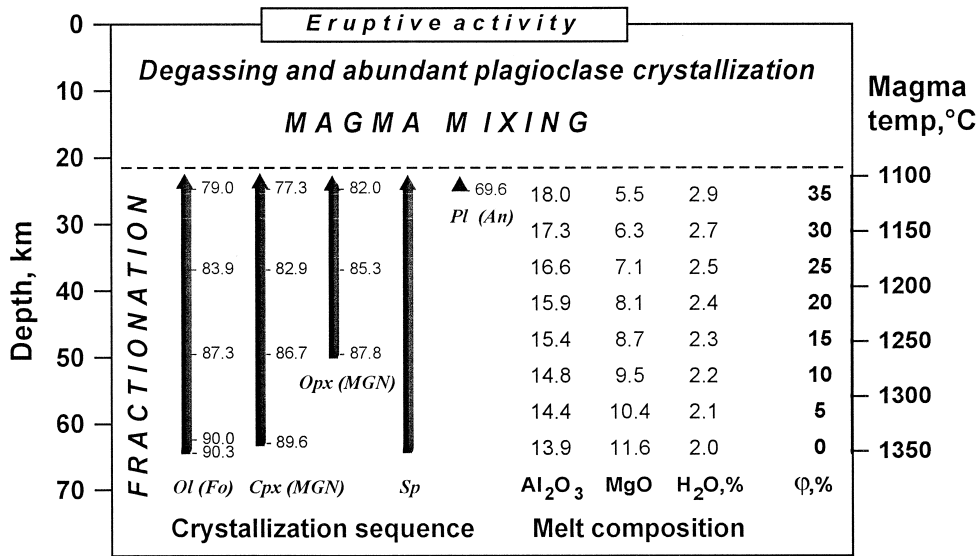


Fig. 20. Modeled crystallization sequence and compositional evolution during decompression fractional crystallization for the average Klyuchevskoi high-Mg basalt as a function of depth, magma temperature and degree of fractionation (ϕ). Conditions of calculations see captions to Fig. 19. This plot demonstrates that HAB melts are formed at the depths of 20 km. At higher levels these melts take part in the processes of mixing with other (even more primitive) differentiates and undergo abundant Pl crystallization due to degassing of water, generating observed varieties of high-alumina, alumina, and probably magnesian basalts.

HMB liquid is 36% and the modeled residual melt is compositionally similar to the Klyuchevskoi high-alumina basalts (Figs. 19 and 20) (Ariskin et al., 1995).

4.4. Significance of the modeling for the problem of origin of high-Al basalts

The proposed model of decompression fractionation of a parental high-magnesia magma may be considered as a plausible mechanism responsible for the formation of subduction zone high-Al basalts. A key aspect of this model is the decrease in pressure during crystallization, which allows a multiply saturated mafic mineral assemblage to fractionate over a wide range of pressures, which depends mostly upon the contents of MgO and CaO in the parental HMB magma. In the case of Klyuchevskoi basalts, these pressures range approximately from 19 to 7 kbar. As was mentioned in Section 2.2.4, the use of the polybaric version of COMAGMAT may result in a misfit of 2–3 kbar: this accuracy of the phase equilibria calculations should be kept in mind during geological interpretations of the results obtained.

Another important factor of the proposed model is a monotonous increase in water content, from approximately 2 to 3 wt.%, which results in a considerable delay of Pl crystallization and the formation of high-alumina differentiates containing at least 18 wt.% Al₂O₃. It is interesting that independent estimates of water contents in melt inclusions observed in olivines from Klyuchevskoi magnesian basalts indicate 1.85% H₂O at 10.3% MgO and 2.46% H₂O at 8.8% MgO in the trapped melts (Sobolev and Chaussidon, 1996). These estimates were obtained by ion microprobe and are in good agreement with the results of computer modeling indicating 2 wt.% water in the initial HMB liquid (Fig. 20).

4.4.1. Dynamic interpretation of the decompression modeling

The decompression model is principally a thermodynamic model indicating the range of external conditions under which the proposed parental melt might pass from one state, corresponding to a high-magnesia magma, to another state, corresponding to the observed compositions of high-alumina basalts. Thus,

it cannot be regarded as an all-embracing model of the magmatic evolution of Klyuchevskoi volcano accounting for the complex history of the volcanic centre which probably included mixing between differentiates, magma recharge, as well degassing and eruptions. Dynamics or real physical mechanisms responsible for the proposed fractionation process are incorporated here implicitly—through a parameter characterizing the rate of decompression $dP/d\varphi_{cr}$. It is obvious that the assumed optimum values of $dP/d\varphi_{cr} = -0.33$ kbar/mol%, are related to the speed at which primary Klyuchevskoi magmas would rise to the surface. By this reasoning, the degree of pressure decline per percent crystallized needs to be taken into account when deriving more rigorous dynamic or geophysical models of the evolution of volcanic systems (Ozerov et al., 1996).

4.4.2. Geological interpretation of the decompression modeling

The main geological conclusion which follows from this modeling is concerned with the probable structure of the deep-seated magma conduit under Klyuchevskoi volcano. Chemical evidence for the decompression fractional crystallization of HMB allows us to suggest the absence of conditions for isobaric fractionation, which could proceed if a large magma chamber would exist at depths of more than 20 km. Thus, the decompression model is argued for by the very absence of such a magma chamber under Klyuchevskoi volcano. This phase equilibria constrained conclusion is in general agreement with available seismic data (Fedotov et al., 1990; Ozerov et al., 1997).

Moreover, the results of the decompression modeling indicate there is a point to distinguish a volcanic rock-forming process resulting in the formation of geological bodies on Earth's surface (lava flows, bombs, etc.) from deep fractionation processes responsible for the formation of chemically diverse minerals and glasses constituting the bodies. If this concept is applied to Klyuchevskoi volcano, it is not necessary to oppose magma mixing and crystallization processes: the first one probably predominant at higher levels of the Klyuchevskoi magma column (especially during eruptions), whereas polybaric fractionation was occurred mostly at earlier stages of the magmatic evolution, just after separation of primary

magmas from the mantle source (Ariskin et al., 1995) (Fig. 20).

5. Conclusions

In this paper we presented a new version of COMAGMAT, a phase equilibria model designed for computer simulations of equilibrium, fractional and intermediate crystallization of basaltic magmas at low to high pressures (Ariskin et al., 1987, 1993). Recent modifications of COMAGMAT were discussed including the ability to calculate more accurately the appearance of magnetite and ilmenite on the liquidus, allowing the user to study numerically the effect of oxygen fugacity on magma fractionation trends in the presence of Fe–Ti oxides (Ariskin and Barmina, 1999). This model has an internal precision of about 10–20°C, which commonly provides realistic reproduction of the crystallization sequences and liquid lines of descent during magma crystallization in a wide range of compositions, from magnesian and iron enriched basalts to andesites and dacites.

Based on the thermodynamic and empirical principles of the construction of COMAGMAT, it is strongly recommended that the model be used in combination with the INFOREX experimental database, which now accesses information on 235 experimental studies carried out from 1962 to 1996 and includes 8660 individual runs plus 11,370 coexisting phase compositions (Meshalkin and Ariskin, 1996; Ariskin et al., 1996, 1997). Search functions of INFOREX make it possible to create mineral–melt equilibria datafiles, which could be used further for additional calibration and correction of the COMAGMAT model in a given range of compositions and external conditions.

5.1. Conclusions from the modeling of Skaergaard magma differentiation

Using an improved version of COMAGMAT-3.5 a set of phase equilibria calculations called Geochemical Thermometry (Frenkel et al., 1988a) has been conducted for 6 cumulative rocks from the Marginal Border Series of the Skaergaard intrusion. It allowed us to specify the initial temperature ($1165 \pm 10^\circ\text{C}$) and trapped melt composition, which was

found to be close to the KT chilled gabbro previously proposed to be parental magma to the Skaergaard intrusion (Hoover, 1989). However, results of simulations of perfect fractionation of the two probable ferro-basaltic parents produced petrochemical trends opposite to those followed from natural observations (Wager and Brown, 1967; Brooks and Nielsen, 1978, 1990; McBirney and Naslund, 1990). The ferro-basaltic melts were interpreted to represent trapped liquids which do not resemble initial Skaergaard magma coming with a large amount of olivine and plagioclase crystals. It led us to conclude that the Skaergaard magma fractionation process was controlled by suspended crystals–melt equilibria intermediate between equilibrium and fractional crystallization.

This interpretation implies that the classic Wager's trend should be considered as an exception rather than a rule for the differentiation of ferro-basaltic magmas. This iron enrichment versus silica depletion trend is probably typical of the residual melts separated from highly crystallized systems, which may have been fractionated under closed conditions with respect to oxygen (Ariskin et al., 1988; Toplis and Carroll, 1996).

5.2. Conclusions from the modeling of Klyuchevskoi magma differentiation

A polybaric version of COMAGMAT-3.0 (Ariskin et al., 1993) has been applied for the genetic interpretation of a volcanic suite from the Klyuchevskoi volcano (Kamchatka, Russia). To identify the petrological processes responsible for the observed suite ranging from high-magnesia to high-alumina basalts, we used the COMAGMAT model to simulate the Klyuchevskoi suite assuming isobaric crystallization of a parental HMB magma at a variety of pressures (1 atm, 2, 4, . . . 20 kbar), and a separate set of simulations assuming fractionation during continuous magma ascent from a depth of 60 km. These results indicate that the Klyuchevskoi trend can be produced by ~ 40% fractionation of Ol–Aug–Sp ± Opx assemblages during ascent of the parental HMB magma over the pressure range 19–7 kbar with the rate of decompression being 0.33 kbar/% crystallized (at 1350–1110°C), with ~ 2 wt.% of H₂O in the initial melt and ~ 3 wt.% of H₂O in the resultant high-Al

basalt (Ariskin et al., 1995). The decompression hypothesis is in general agreement with seismic data suggesting the absence of a large magma chamber under Klyuchevskoi volcano (Fedotov et al., 1990; Ozerov et al., 1997).

Acknowledgements

This research was initiated and developed during joint work with the late Mike Frenkel whose ideas on thermodynamics and dynamics of magma differentiation processes constitute the basis of the COMAGMAT model. I am especially grateful to my wife and regular co-author, Galina Barmina, of her long standing help in the field, analytical studies and petrological studies including most of the topics discussed in the paper. Help of Renat Almeev, George Nikolaev and Sergei Meshalkin is also acknowledged. I sincerely thank Evgeny Koptev-Dvornikov and Alexei Ozerov for joint researches dealing with the formation of layered intrusions and volcanic series. I would like also to thank Sergei Khubunaya for his assistance with field work at Eastern Kamchatka and Boris Kireev for organizing expeditions to layered intrusions of Eastern Siberia and Northern Karelia, Russia. Fruitful discussions with Chris Chalokwu, Dana Johnston, Roger Nielsen and Alex Sobolev on different aspects of the topic are greatly acknowledged. Bruce Marsh is particularly thanked for the critical review and help with the translation which considerably improved the manuscript. This research was supported by grants from NSF (EAR 9206647), International Science Foundation (MINOOO), and Russian Foundation of Basic Research (99-05-64875, 96-05-64231, 96-07-89054).

References

- Almeev, R.R., Ariskin, A.A., 1996. Mineral–melt equilibria in a hydrous basaltic system: computer modelling. *Geochem. Int.* 34 (7), 563–573.
- Ariskin, A.A., 1998. Calculation of titanomagnetite stability on the liquidus of basalts and andesites with special reference to tholeiitic magma differentiation. *Geochem. Int.* 36 (1), 15–23.
- Ariskin, A.A., Barmina, G.S., 1990. Equilibria thermometry between plagioclases and basalt or andesite magmas. *Geochem. Int.* 27 (10), 129–134.

- Ariskin, A.A., Barmina, G.S., 1999. An empirical model for the calculation of spinel-melt equilibrium in mafic igneous systems at atmospheric pressure: II. Fe–Ti oxides. *Contrib. Mineral. Petrol.* 134, 251–263.
- Ariskin, A.A., Nielsen, R.L., 1993. Application of computer simulation of magmatic processes to the teaching of petrology. *J. Geol. Educ.* 41, 438–441.
- Ariskin, A.A., Barmina, G.S., Frenkel, M.Ya., 1987. Computer simulation of basalt magma crystallization at a fixed oxygen fugacity. *Geochem. Int.* 24 (6), 85–98.
- Ariskin, A.A., Barmina, G.S., Frenkel, M.Ya., Yaroshevsky, A.A., 1988. Simulating low-pressure tholeiite-magma fractional crystallization. *Geochem. Int.* 25 (4), 21–37.
- Ariskin, A.A., Frenkel, M.Ya., Tsekhonya, T.I., 1990. High-pressure fractional crystallization of tholeiitic magmas. *Geochem. Int.* 27 (9), 10–20.
- Ariskin, A.A., Frenkel, M.Ya., Barmina, G.S., Nielsen, R.L., 1993. COMAGMAT: a Fortran program to model magma differentiation processes. *Comput. Geosci.* 19, 1155–1170.
- Ariskin, A.A., Barmina, G.S., Ozerov, A.Yu., Nielsen, R.L., 1995. Genesis of high-alumina basalts from Klyuchevskoi volcano. *Petrology* 3, 449–472.
- Ariskin, A.A., Barmina, G.S., Meshalkin, S.S., Nikolaev, G.S., Almeev, R.R., 1996. INFOREX-3.0: A database on experimental phase equilibria in igneous rocks and synthetic systems: II. Data description and petrological applications. *Comput. Geosci.* 22, 1073–1082.
- Ariskin, A.A., Meshalkin, S.S., Almeev, R.R., Barmina, G.S., Nikolaev, G.S., 1997. INFOREX information retrieval system: analysis and processing of experimental data on phase equilibria in igneous rocks. *Petrology* 5, 28–36.
- Babansky, A.D., Ryabchikov, I.D., Bogatkov, O.A., 1983. The Evolution of Calc-alkaline Magmas. Nauka, Moscow, USSR, 96 pp. (in Russian).
- Baker, D.R., Eggler, D.H., 1983. Fractionation paths of Atka (Aleutian) high-alumina basalts: constraints from phase relations. *J. Volcanol. Geotherm. Res.* 18, 387–404.
- Barmina, G.S., Ariskin, A.A., Frenkel, M.Ya., Kononkova, N.N., 1988. Origin of the Chazhma-sill ferrodiorites. *Geochem. Int.* 25 (5), 110–114.
- Barmina, G.S., Ariskin, A.A., Frenkel, M.Ya., 1989a. Petrochemical types and crystallization conditions of the Kronotsky Peninsula plagioclolerite (Eastern Kamchatka). *Geochem. Int.* 26 (9), 24–37.
- Barmina, G.S., Ariskin, A.A., Koptev-Dvornikov, E.V., Frenkel, M.Ya., 1989b. Estimates of the primary compositions of cumulate-minerals in differentiated traps. *Geochem. Int.* 26 (3), 32–42.
- Barmina, G.S., Ariskin, A.A., Kolesov, G.M., 1992. Simulating the REE spectra of hypabyssal rocks in the Kronotsky series, Eastern Kamchatka. *Geochem. Int.* 29 (3), 45–54.
- Bender, J.F., Hodges, F.N., Bence, A.E., 1978. Petrogenesis of basalts from the Project Famous Area: experimental study from 0 to 15 kbars. *Earth Planet. Sci. Lett.* 41, 277–302.
- Bergantz, G.W., 1995. Changing techniques and paradigms for the evaluation of magmatic processes. *J. Geophys. Res.* 100, 17603–17613.
- Biggar, G.M., 1983. Crystallization of plagioclase, augite, and olivine in synthetic systems and in tholeiites. *Mineral. Mag.* 47, 161–176.
- Bolikhovskaya, S.V., Vasil'yeva, M.O., Koptev-Dvornikov, E.V., 1996. Simulating low-Ca pyroxene crystallization in basite systems: new geothermometer versions. *Geochem. Int.* 33 (12), 1–19.
- Boudreau, A.E., McBirney, A.R., 1997. The Skaergaard Layered Series: Part III. Non-dynamic layering. *J. Petrol.* 38, 1003–1020.
- Bowen, N.L., 1928. *The Evolution of the Igneous Rocks*. Princeton Univ. Press, Princeton, NJ, 334 pp.
- Brooks, C.K., Nielsen, T.F.D., 1978. Early stages in the differentiation of the Skaergaard magma as revealed by a closely related suite of dike rocks. *Lithos* 11, 1–14.
- Brooks, C.K., Nielsen, T.F.D., 1990. The differentiation of the Skaergaard intrusion. A discussion of Hunter and Sparks (*Contrib. Mineral. Petrol.* 95: 451–461). *Contrib. Mineral. Petrol.* 104, 244–247.
- Brooks, C.K., Larsen, L.M., Nielsen, T.F.D., 1991. Importance of iron-rich tholeiitic magmas at divergent plate margins: a reappraisal. *Geology* 19, 269–272.
- Brophy, J.G., 1988. Basalt convection and plagioclase retention: a model for the generation of high-alumina basalt. *J. Geol.* 97, 319–329.
- Brophy, J.G., Marsh, B.D., 1986. On the origin of high-alumina arc basalt and the mechanics of melt extraction. *J. Petrol.* 27, 763–789.
- Camur, M.Z., Kilinc, A.I., 1995. Empirical solution model for alkaline to tholeiitic basic magmas. *J. Petrol.* 36, 497–514.
- Carmichael, I.S.E., 1964. The petrology of Thingmuli, a Tertiary volcano in Eastern Island. *J. Petrol.* 5, 435–460.
- Chalokwu, C.I., Grant, N.K., Ariskin, A.A., Barmina, G.S., 1993. Simulation of primary phase relations and mineral compositions in the Partridge River intrusion, Duluth Complex, Minnesota: implications for the parent magma composition. *Contrib. Mineral. Petrol.* 114, 539–549.
- Chalokwu, C.I., Ariskin, A.A., Koptev-Dvornikov, E.V., 1996. Forward modeling of the incompatible element enrichment at the base of the Partridge River intrusion, Duluth Complex, Minnesota: Magma dynamics in a lower mushy zone. *Geochim. Cosmochim. Acta* 60, 4997–5011.
- Crawford, A.J., Falloon, T.J., Eggins, S., 1987. The origin of island arc high-alumina basalts. *Contrib. Mineral. Petrol.* 97, 417–430.
- Cribb, J.W., Barton, M., 1996. Geochemical effects of decoupled fractional crystallization and crustal assimilation. *Lithos* 37, 293–307.
- DePaolo, D.J., 1981. Trace element and isotopic effects of combined wallrock assimilation and fractional crystallization. *Earth Planet. Sci. Lett.* 53, 189–202.
- Dixon, J.E., Stolper, E.M., Holloway, J.R., 1995. An experimental study of water and carbon dioxide solubilities in mid-ocean ridge basaltic liquids. Part 1: Calibration and solubility models. *J. Petrol.* 36, 1607–1631.
- Draper, D.S., Johnston, A.D., 1992. Anhydrous PT phase relations of an Aleutian high-MgO basalt: an investigation of the role of

- olivine–liquid reaction in the generation of arc high-alumina basalts. *Contrib. Mineral. Petrol.* 112, 501–519.
- Eggler, D.H., Osborn, E.F., 1982. Experimental studies of the system $\text{MgO-FeO-Fe}_2\text{O}_3\text{-NaAlSi}_3\text{O}_8\text{-CaAl}_2\text{Si}_2\text{O}_8\text{-SiO}_2$ — a model for subalkaline magmas. *Am. J. Sci.* 282, 1012–1041.
- Fedotov, S.A., Khrenov, A.P., Zharinov, N.A., 1990. The activity of Klyuchevskoi volcano in the years 1932–1986 and the prospects for the future. *Volcanol. Seismol.* 9 (4), 501–521.
- Fournelle, J., Marsh, B.D., 1991. Shisalkin volcano: Aleutian high-alumina basalts and the question of plagioclase accumulation. *Geology* 19, 234–237.
- Frenkel, M.Ya., Ariskin, A.A., 1984. A computer algorithm for equilibration in a crystallizing basalt magma. *Geochem. Int.* 21 (5), 63–73.
- Frenkel, M.Ya., Ariskin, A.A., Barmina, G.S., Korina, M.I., Koptev-Dvornikov, E.V., 1988a. Geochemical thermometry of magmatic rocks—principles and example. *Geochem. Int.* 25 (6), 35–50.
- Frenkel, M.Ya., Yaroshevsky, A.A., Ariskin, A.A., Barmina, G.S., Koptev-Dvornikov, E.V., Kireev, B.S., 1988b. Dynamics of in situ Differentiation of Mafic Magmas. Nauka, Moscow, USSR, 216 pp. (in Russian).
- Frenkel, M.Ya., Yaroshevsky, A.A., Ariskin, A.A., Barmina, G.S., Koptev-Dvornikov, E.V., Kireev, B.S., 1989. Convective–cumulative model simulating the formation process of stratified intrusions. In: Bonin, B., Didier, J., Le Fort, P., Propach, G., Puga, E., Vistelius, A.B. (Eds.), *Magma–Crust Interactions and Evolution*. Theophrastus Publications, Athens, Greece, pp. 3–88.
- Ghiorso, M.S., 1985. Chemical mass transfer in magmatic processes I. Thermodynamic relations and numeric algorithms. *Contrib. Mineral. Petrol.* 90, 107–120.
- Ghiorso, M.S., 1997. Thermodynamic models of igneous processes. *Annu. Rev. Earth Planet. Sci.* 25, 221–241.
- Ghiorso, M.S., Carmichael, I.S.E., 1985. Chemical mass transfer in magmatic processes: II. Applications in equilibrium crystallization, fractionation and assimilation. *Contrib. Mineral. Petrol.* 90, 121–141.
- Ghiorso, M.S., Sack, R.O., 1995. Chemical mass transfer in magmatic processes: IV. A revised and internally consistent thermodynamic model for the interpolation and extrapolation of liquid–solid equilibria in magmatic systems at elevated temperatures and pressures. *Contrib. Mineral. Petrol.* 119, 197–212.
- Grove, T.L., 1993. Corrections to expressions for calculating mineral-components in ‘Origin of calc-alkaline series lavas at Medicine Lake volcano by fractionation, assimilation and mixing’ and ‘Experimental petrology of normal MORB near the Kane Fracture Zone: 22°–25°N, mid-Atlantic ridge’. *Contrib. Mineral. Petrol.* 114, 422–424.
- Grove, T.L., Baker, M.B., 1984. Phase equilibrium controls on the tholeiitic versus calc-alkaline differentiation trends. *J. Geophys. Res.* 89B, 3253–3274.
- Grove, T.L., Bryan, W.B., 1983. Fractionation of pyroxene–phyric MORB at low pressure: an experimental study. *Contrib. Mineral. Petrol.* 84, 293–309.
- Grove, T.L., Kinzler, R.J., 1986. Petrogenesis of andesites. *Annu. Rev. Earth. Planet. Sci.* 14, 417–454.
- Grove, T.L., Gerlach, D.C., Sando, T.W., 1982. Origin of calc-alkaline series lavas at Medicine Lake volcano by fractionation, assimilation and mixing. *Contrib. Mineral. Petrol.* 80, 160–182.
- Grove, T.L., Kinzler, R.J., Bryan, W.B., 1990. 2. Natural and experimental phase relations of lavas from Serocki volcano. *Proc. Ocean Drilling Program. Scientific Results* 106/109, 9–17.
- Gust, D.A., Perfit, M.R., 1987. Phase relations on a high-Mg basalt from the Aleutian Island Arc: implications for primary island arc basalts and high-Al basalts. *Contrib. Mineral. Petrol.* 97, 7–18.
- Hamilton, D.L., Burnham, C.W., Osborn, E.F., 1964. The solubility of water and effects of oxygen fugacity and water content on crystallization in mafic magmas. *J. Petrol.* 5, 21–39.
- Hill, R., Roeder, P., 1974. The crystallization of spinel from basaltic liquid as a function of oxygen fugacity. *J. Geol.* 82, 709–729.
- Hoover, J.D., 1989. The chilled marginal gabbro and other contact rocks of the Skaergaard intrusion. *J. Petrol.* 30, 441–476.
- Hunter, R.H., Sparks, R.S.J., 1987. The differentiation of the Skaergaard intrusion. *Contrib. Mineral. Petrol.* 95, 451–461.
- Hunter, R.H., Sparks, R.S.J., 1990. The differentiation of the Skaergaard intrusion. Replies to A.R. McBirney and H.R. Naslund, to S.A. Morse, to C.K. Brooks and T.F.D. Nielsen. *Contrib. Mineral. Petrol.* 104, 248–254.
- Irvine, T.N., 1980. Magmatic infiltration metasomatism, double-diffusive fractional crystallization, and accumulation growth in the Maskox intrusion and other layered intrusions. In: Hargraves, R.B. (Ed.), *Physics of Magmatic Processes*. Princeton Univ. Press, Princeton, NJ, pp. 325–384.
- Jaupart, C., Tait, S., 1995. Dynamics of differentiation in magma reservoirs. *J. Geophys. Res.* 100, 17615–17636.
- Johnston, A.D., 1986. Anhydrous P – T phase relations of near-primary high-alumina basalt from the South Sandwich Islands: implications for the origin of island arcs and tonalite–trondhjemite. *Contrib. Mineral. Petrol.* 92, 24–38.
- Kadik, A.A., Lebedev, E.B., Khitarov, N.I., 1971. *Water in Magmatic Melts*. Nauka, Moscow, USSR, 210 pp. (in Russian).
- Kadik, A.A., Maksimov, A.P., Ivanov, B.V., 1986. *Physical–Chemical Conditions of Crystallization and the Genesis of Andesites*. Nauka, Moscow, USSR, 158 pp. (in Russian).
- Kadik, A.A., Lukanin, O.A., Lapin, I.V., 1990. *Physical–Chemical Conditions of the Evolution of Basalt Magmas in the Shallow Chambers*. Nauka, Moscow, USSR, 346 pp. (in Russian).
- Kay, S.M., Kay, R.W., 1985. Aleutian tholeiitic and calc-alkaline magma series: I. the mafic phenocrysts. *Contrib. Mineral. Petrol.* 90, 276–296.
- Kelemen, P.B., 1990. Reaction between ultramafic rock and fractionating basalt magma: I. Phase relations, the origin of calc-alkaline magma series, and the formation of discordant dunite. *J. Petrol.* 31, 51–98.
- Kersting, A.B., Arculus, R.J., 1994. Klyuchevskoy volcano, Kamchatka, Russia: the role of high-flux recharge, tapped, and fractionated magma chamber(s) in the genesis of high- Al_2O_3 from high-MgO basalt. *J. Petrol.* 35, 1–41.
- Khrenov, A.P., Antipin, V.S., Chuvashova, L.A., Smirnova, E.V.,

1990. Petrochemistry and geochemistry of Klyuchevskoi basalts. *Volcanol. Seismol.* 11 (3), 285–304.
- Kuno, H., 1960. High-alumina basalt. *J. Petrol.* 1, 121–145.
- Longhi, J., 1991. Comparative liquidus equilibria of hypersthene–normative basalts at low pressure. *Am. Mineral.* 76, 785–800.
- Maaloe, S., 1976. Quantitative aspects of fractional crystallization of major elements. *J. Geol.* 84, 81–96.
- Marsh, B.D., 1989. Magma chambers. *Annu. Rev. Earth Planet. Sci.* 17, 439–474.
- Marsh, B.D., 1995. The 1995 Hallimond lecture. Solidification fronts and magmatic evolution. *Mineral. Mag.* 60, 5–40.
- McBirney, A.R., 1989. The Skaergaard Layered Series: I. Structure and average compositions. *J. Petrol.* 30, 363–397.
- McBirney, A.R., 1996. The Skaergaard Intrusion. In: Cawthorn, R.J. (Ed.), *Layered Intrusions*. Elsevier Science, pp. 147–180.
- McBirney, A.R., Nakamura, Y., 1974. Immiscibility in late-stage of the Skaergaard intrusion. *Carnegie Institute Washington Yearbook* 72, 348–352.
- McBirney, A.R., Naslund, H.R., 1990. The differentiation of the Skaergaard intrusion. A discussion of Hunter and Sparks (Contrib Mineral Petrol 95: 451–461). *Contrib. Mineral. Petrol.* 104, 235–240.
- Meshalkin, S.S., Ariskin, A.A., 1996. INFOREX-3.0: a database on experimental phase equilibria in igneous rocks and synthetic systems: I. Datafile and management system structure. *Comput. Geosci.* 22, 1061–1071.
- Morse, S.A., 1981. Kiglapait geochemistry: IV. the major elements. *Geochim. Cosmochim. Acta* 45, 461–479.
- Morse, S.A., 1990. The differentiation of the Skaergaard intrusion. A discussion of Hunter and Sparks (Contrib Mineral Petrol 95: 451–461). *Contrib. Mineral. Petrol.* 104, 240–244.
- Myers, J.D., Johnston, A.D., 1996. Phase equilibria constraints on models of subduction zone magmatism. In: Bebout, G.E., Scholl, D.W., Kirby, S.H., Platt, J.P. (Eds.), *Subduction Top to Bottom*. Geophys. Monograph, Vol. 96, pp. 229–249.
- Naslund, H.R., McBirney, A.R., 1996. Mechanisms of formation of igneous layering. In: Cawthorn, R.J. (Ed.), *Layered Intrusions*, Elsevier Science, pp. 1–43.
- Nielsen, R.L., 1990. Simulation of igneous differentiation processes. In: Nicholls, J., Russell, J.K. (Eds.), *Modern Methods of Igneous Petrology: Understanding Magmatic Processes, Reviews in Mineralogy*, Vol. 24, pp. 63–105.
- Nielsen, R.L., Dungan, M.A., 1983. Low-pressure mineral–melt equilibria in natural anhydrous mafic systems. *Contrib. Mineral. Petrol.* 84, 310–326.
- Nye, C.J., Reid, M.R., 1986. Geochemistry of primary and least fractionated lavas from Okmok volcano, central Aleutians: implications for arc magma genesis. *J. Geophys. Res.* 91, 10271–10287.
- O'Hara, M.J., Mathews, R.E., 1981. Geochemical evolution in an advancing, periodically replenished, periodically tapped, continuously fractionating magma chamber. *J. Geol. Soc. London* 138, 237–277.
- Osborn, E.F., 1959. Role of oxygen pressure in the crystallization and differentiation of basaltic magma. *Am. J. Sci.* 257, 609–647.
- Osborn, E.F., 1979. The reaction principle. In: Yoder, H.S., Jr. (Ed.), *The Evolution of the Igneous Rocks: 50th Anniversary Perspective*. Princeton Univ. Press, Princeton, NJ, pp. 133–169.
- Ozerov, A.Yu., Ariskin, A.A., Barmina, G.S., 1996. The problem of genetic relations between high-alumina and high-magnesia basalts of the Klyuchevskoi volcano. *Kamchatka. Trans. Rus. Acad. Sci.* 350 (7), 1127–1130.
- Ozerov, A.Yu., Ariskin, A.A., Kyle, P., Bogoyavlenskaya, G.E., Karpenko, S.F., 1997. Petrological–geochemical model for genetic relationships between basaltic and andesitic magmatism of Klyuchevskoi and Bezmyannii volcanoes. *Kamchatka. Petrol.* 5, 550–569.
- Perfit, M.R., Gust, D.A., Bence, A.E., Arculus, R.J., Taylor, S.R., 1980. Chemical characteristics of island-arc basalts: implications for mantle sources. *Chem. Geol.* 30, 227–256.
- Plank, T., Langmuir, C.H., 1988. An evaluation of the global variations in the major element chemistry of arc basalts. *Earth Planet. Sci. Lett.* 90, 349–370.
- Presnall, D.C., 1966. The join forsterite–diopside–iron oxide and its bearing on the crystallization of basaltic and ultramafic magmas. *Am. J. Sci.* 264, 753–809.
- Sack, R.O., Carmichael, I.S.E., Rivers, M., Ghiorso, M.S., 1980. Ferric–ferrous equilibria in natural silicate liquids at 1 bar. *Contrib. Mineral. Petrol.* 75, 369–376.
- Sakuyama, M., 1981. Petrological study of the Myoko and Kurohime volcanoes, Japan: crystallization sequence and evidence for magma mixing. *J. Petrol.* 22, 553–583.
- Shi, P., 1993. Low-pressure phase relationships in the system $\text{Na}_2\text{O}-\text{CaO}-\text{FeO}-\text{MgO}-\text{Al}_2\text{O}_3-\text{SiO}_2$ at 1100°C, with implications for the differentiation of basaltic magmas. *J. Petrol.* 34, 743–762.
- Sisson, T.W., Grove, T.L., 1993a. Experimental investigations of the role of H_2O in calc–alkaline differentiation and subduction zone magmatism. *Contrib. Mineral. Petrol.* 113, 143–166.
- Sisson, T.W., Grove, T.L., 1993b. Temperatures and H_2O contents of low-MgO high-alumina basalts. *Contrib. Mineral. Petrol.* 113, 167–184.
- Snyder, D., Carmichael, I.S.E., Wiebe, R.A., 1993. Experimental study of liquid evolution in an Fe-rich, layered mafic intrusion: Constraints of Fe–Ti oxide precipitation on the $T-f_{\text{O}_2}$ and T-p paths of tholeiitic magmas. *Contrib. Mineral. Petrol.* 113, 73–86.
- Sobolev, A.V., Chaussidon, M., 1996. H_2O concentrations in primary melts from supra–subduction zones and mid-ocean ridges: implications for H_2O storage and recycling in the mantle. *Earth Planet. Sci. Lett.* 137, 45–55.
- Stormer, J.C. Jr., 1983. The effects of recalculation on estimates of temperature and oxygen fugacity from analyses of multi-component iron–titanium oxides. *Am. Mineral.* 68, 586–594.
- Tatsumi, Y., 1982. Origin of high-magnesian andesites in the Setouchi volcanic belt, southwest Japan: II. Melting phase relations at high pressures. *Earth Planet. Sci. Lett.* 60, 305–317.
- Tatsumi, Y., Sakuyama, M., Fukuyama, H., Kushiro, I., 1983. Generation of arc basalt magmas and thermal structure of the mantle wedge in subduction zones. *J. Geophys. Res.* 88, 5815–5825.
- Thy, P., Lofgren, G.E., 1994. Experimental constraints on the

- low-pressure evolution of transitional and mildly alkalic basalts: the effect of Fe–Ti oxide minerals and the origin of basaltic andesites. *Contrib. Mineral. Petrol.* 116, 340–351.
- Toplis, M.J., Carroll, M.R., 1995. An experimental study of the influence of oxygen fugacity on Fe–Ti oxide stability, phase relations, and mineral–melt equilibria in ferro-basaltic systems. *J. Petrol.* 36, 1137–1170.
- Toplis, M.J., Carroll, M.R., 1996. Differentiation of ferro-basaltic magmas under conditions open and closed to oxygen: implications for Skaergaard intrusion and other natural systems. *J. Petrol.* 37, 837–858.
- Torney, D.R., Grove, T.L., Bryan, W.B., 1987. Experimental petrology of normal MORB near the Kane Fracture Zone: 22°–25° N, mid-Atlantic ridge. *Contrib. Mineral. Petrol.* 96, 121–139.
- Uto, K., 1986. Variation of Al₂O₃ content in Late Cenozoic Japanese basalts: a reexamination of Kuno's High-Alumina Basalt. *J. Volcanol. Geotherm. Res.* 29, 397–411.
- Wager, L.R., Deer, W.A., 1939. Geological investigations in East Greenland: Part III. The petrology of the Skaergaard intrusion. *Kangerdlugssuaq, East Greenland, Meddelelser om Gronland* 105 (4), 1–352.
- Wager, L.R., Brown, G.M., 1967. *Layered Igneous Rocks*: San Francisco, Freeman, W.H., 588 pp.
- Walker, D., Shibata, T., DeLong, S.E., 1979. Abyssal tholeiites from the Oceanographer Fracture Zone: II. Phase equilibria and mixing. *Contrib. Mineral. Petrol.* 70, 111–125.
- Weaver, J.S., Langmuir, C.H., 1990. Calculation of phase equilibrium in mineral–melt systems. *Comput. Geosci.* 16, 1–19.
- Yang, H.-J., Kinzler, R.J., Grove, T.L., 1996. Experiments and models of anhydrous, basaltic olivine–plagioclase–augite saturated melts from 0.001 to 10 kbar. *Contrib. Mineral. Petrol.* 124, 1–18.
- Yoder, H.S., Tilley, C.E., 1962. Origin of basalt magmas: an experimental study of natural and synthetic rock systems. *J. Petrol.* 3, 342–352.